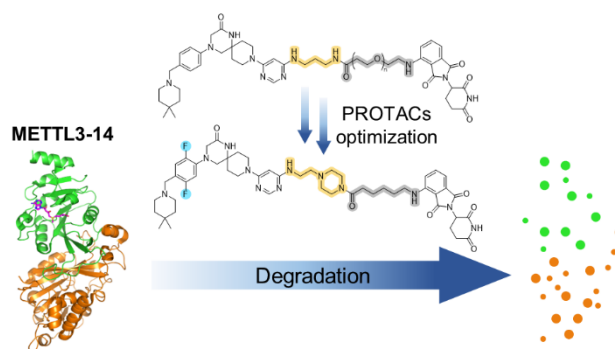


PROTAC degraders of the METTL3-14 m⁶A-RNA methyltransferase

Francesco Errani[§], Annalisa Invernizzi[§], Marcin Herok, Elena Bochenkova, Fiona Stamm, Ivan Corbeski, Valeria Romanucci, Giovanni Di Fabio, František Zálešák*, Amedeo Caflisch*

KEYWORDS: PROTACs, METTL3, METTL14, CRBN, degradation, m⁶A-RNA, AML, prostate cancer.

ABSTRACT: Methylation of adenine N6 (m⁶A) is the most frequent RNA modification. On mRNA, it is catalyzed by the METTL3-14 heterodimer complex which plays a key role in acute myeloid leukemia (AML) and other types of blood cancers and solid tumors. Here we disclose the first proteolysis targeting chimeras (PROTACs) for an epitranscriptomics target. For designing the PROTACs we made use of the crystal structure of the complex of METTL3-14 with a potent and selective small-molecule inhibitor (called UZH2). The optimization of the linker started from a desfluoro precursor of UZH2 whose synthesis is more efficient than the one of UZH2. The first nine PROTAC molecules featured PEG- or alkyl-based linkers but only the latter showed cell penetration. With this information in hand, we synthesized 26 PROTACs based on UZH2 and alkylic linkers of different lengths and rigidity. The formation of the ternary complex was validated by a FRET-based biochemical assay and an *in vitro* ubiquitination assay. Three PROTACs with three different rigid extensions of UZH2 showed 50% or higher degradation of METTL3 and METTL14 measured by Western blot in MOLM-13. Substantial degradation was measured also on three others AML cell lines and the prostate cancer cell line PC3.



Introduction

Post-transcriptional (epitranscriptomic) modifications of RNA have a key role in gene expression and cell homeostasis regulation.^{1,2} The N6-adenosine methylation (m⁶A) is the most abundant among over 150 reported modifications.³ It has been found on mRNA, tRNA, rRNA and several noncoding RNAs.⁴ The m⁶A is a dynamic and reversible modification deposited by proteins defined as “writers” and removed by “eraser” proteins. A third family of epitranscriptomic proteins (“readers”) recognize the methylated RNA, leading to splicing, nuclear export, translation, altered stability and degradation of transcripts.⁵⁻⁹ In this way, the m⁶A modification can mediate the expression or silencing of specific genes.²

This epitranscriptomic machinery enables processes such as stem cell differentiation¹⁰, cell response to stress¹¹, and regulation of the circadian cycle¹² under physiological conditions. Its dysregulation has been linked to a growing amount of pathological conditions. In particular, abnormal m⁶A levels have been connected to different kinds of cancer including leukemia, prostate cancer, breast cancer, liver cancer, colorectal cancer, and others.¹³⁻²⁰

Methyltransferase-like 3 (METTL3) and METTL14 form the heterodimeric protein complex that catalyses the deposition of the m⁶A modification (writer). METTL3 is the catalytic subunit which binds the co-substrate S-adenosyl-L-methionine (SAM) while METTL14 facilitates RNA binding and stabilization of the complex.^{21,22} Many studies show that increased m⁶A levels can lead to enhanced cell proliferation, antiapoptotic effects, promotion of migration and invasion.²³ Moreover, METTL3 has been reported to promote other cancerogenic processes independently of its catalytic activity.²⁴ This makes the METTL3-14 complex an interesting therapeutic target for anti-cancer drugs.

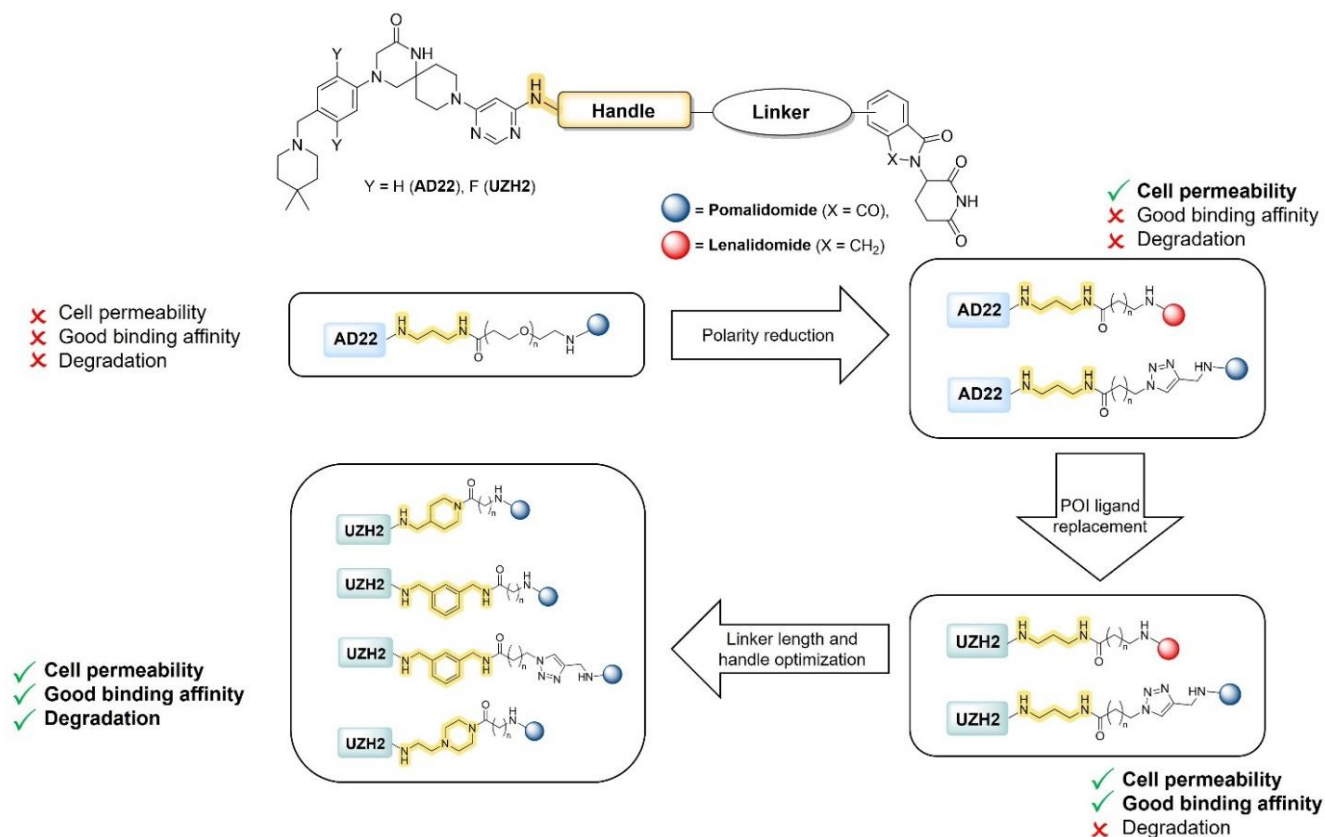
To date, only three series of SAM-competitive, potent and selective inhibitors of METTL3 have been reported, two of them originating from medicinal chemistry campaigns carried out in our group at the University of Zurich (UZH).²⁵⁻²⁸ The low nanomolar inhibitors UZH2 and the compound published by Storm Therapeutics (STM2457) have shown antiproliferative effects in acute myeloid leukemia (AML) cell lines, strengthening the therapeutic potential of targeting the METTL3-14 complex.^{25,27} However, the high cellular concentration of SAM (60 to 160 μ M as measured in rat liver)²⁹ can limit the scope of SAM-competitive inhibitors.

Proteolysis targeting chimeras (PROTACs) are a valid alternative to small-molecule inhibitors.^{30–33} PROTACs are heterobifunctional molecules bearing a protein of interest (POI) ligand covalently linked to an E3 ligase ligand. Upon binding to both targets, PROTACs promote the ubiquitination of the POI and its subsequent degradation by the 26S-proteasome. This is a promising approach already applied to a variety of targets, in particular in the epigenetic field.³⁴ Their catalytic-like mechanism of action results in the recycling/re-use of the PROTAC molecules upon protein

degradation. Moreover, thanks to the degradation of the whole protein, PROTACs eliminate both its enzymatic and scaffolding functions.

Here, we report a medicinal chemistry campaign that aimed at the development of PROTAC molecules against METTL3-14, the human m⁶A-RNA writer complex. To the best of our knowledge, there are currently no degraders in the literature for proteins involved in epitranscriptomics.

Scheme 1. General structure of PROTACs and optimization strategy.



Results and discussion

Protein structure-based design

The medicinal chemistry campaign builds upon our previous results obtained during the development of small molecule inhibitors for METTL3-14.²⁵ Here, we start from two potent and selective METTL3-14 inhibitors, UZH2 (IC₅₀ = 5 nM, selectivity data in Table S1) and its desfluoro derivative AD22 (IC₅₀ = 89 nM, compound **10** in Ref.²⁵) (Figure 1A). As E3 ubiquitin ligase, we selected Cereblon (CRBN), for which the most common ligands are 4-amino thalidomide (pomalidomide) and lenalidomide.^{35,36} The general structure of the synthesized PROTACs is represented in Scheme 1. The UZH2/AD22 atom for the covalent bond with the linker was identified from crystallographic analysis. The binding poses of UZH2 (PDB 702F) and AD22 (PDB 700P) in the METTL3-14 complex (Figure 1B) provide an exit vector from the pyrimidine ring into the solvent-exposed area. Replacing the

methylamino moiety with a propyl diamino motif (handle) allowed a convenient connection to the CRBN ligand via a linker. The amino group directly connected to the pyrimidine ring was intended to maintain a favorable hydrogen bond interaction with the side chain of Asp377 in METTL3 (Figure 1C). The terminal amino functionality allowed the final amide bond formation, thus connecting the POI ligand with pomalidomide through the linker (Scheme 1). The propyl diamino moiety is formally considered part of the linker. Nevertheless, it affects the affinity of the PROTACs for METTL3-14 as measured in our time-resolved FRET assay (hereafter referred to as binary assay).³⁷ For this reason, this portion is called “handle”, to clearly distinguish it from the rest of the linker. The structures of all the synthesized PROTACs (compounds 1-35) are reported in Table 1. The first set of PROTAC molecules (compounds 1-4) consists of AD22 as POI ligand, propyl diamine handle, polyethylene glycol (PEG) linker, and pomalidomide as the E3 ligase binder. Their synthesis was achieved by a final amide bond

formation, as described in further detail in Scheme 4 in the synthesis section.

The rationale behind the use of PEG linkers in the first generation was the commercial availability of PEG chains with different numbers of PEG subunits.³⁸ This allowed us to cover different distances between the PROTAC moieties for POI and CRBN. This is useful for investigating the optimal range for the formation of the ternary complex CRBN/PROTAC/METTL3-14. Moreover, the PEG chain is widely used in cross-linking for bioconjugation and bio-labeling, due to its favorable physicochemical properties.³⁹⁻⁴¹ The degradation of METTL3 and METTL14 was measured individually by Western blot at various PROTAC concentrations (10, 5, 1, 0.1, 0.01 μM) at 16h time point, in MOLM-13 which is an AML cell line. However, none of the four first generation PROTACs (compounds 1-4) showed degradation activity. Compounds 1, 2, 3 and 4 were also tested in a

biochemical ternary complex formation assay (TCFA).⁴² Relatively high effective concentrations at the peak of the Hook curve (EC_{max} : 6.8 μM , 2.8 μM , 1.9 μM and 2.0 μM , respectively) reflect low affinity towards both CRBN and METTL3-14. In addition, the amplitude of the Hook curve (Table S2) is low compared to other compounds in this paper. This can be an indication of weak cooperativity and less stable ternary complex formation, which is needed for successful degradation activity.⁴³ As PROTACs can suffer from low cellular permeability due to their high molecular weight and/or high hydrophilicity,⁴⁴ we decided to assess permeability and target engagement in cells using the cellular thermal shift assay (CETSA).⁴⁵ The first set of PROTACs (compounds 1-4) exhibited low protein stabilization, and only at the very high concentration of 100 μM . Considering the CETSA (Figure 2) and TCFA results, the lack of degradation might be a result of low cell permeability and/or inability to form a stable ternary complex.

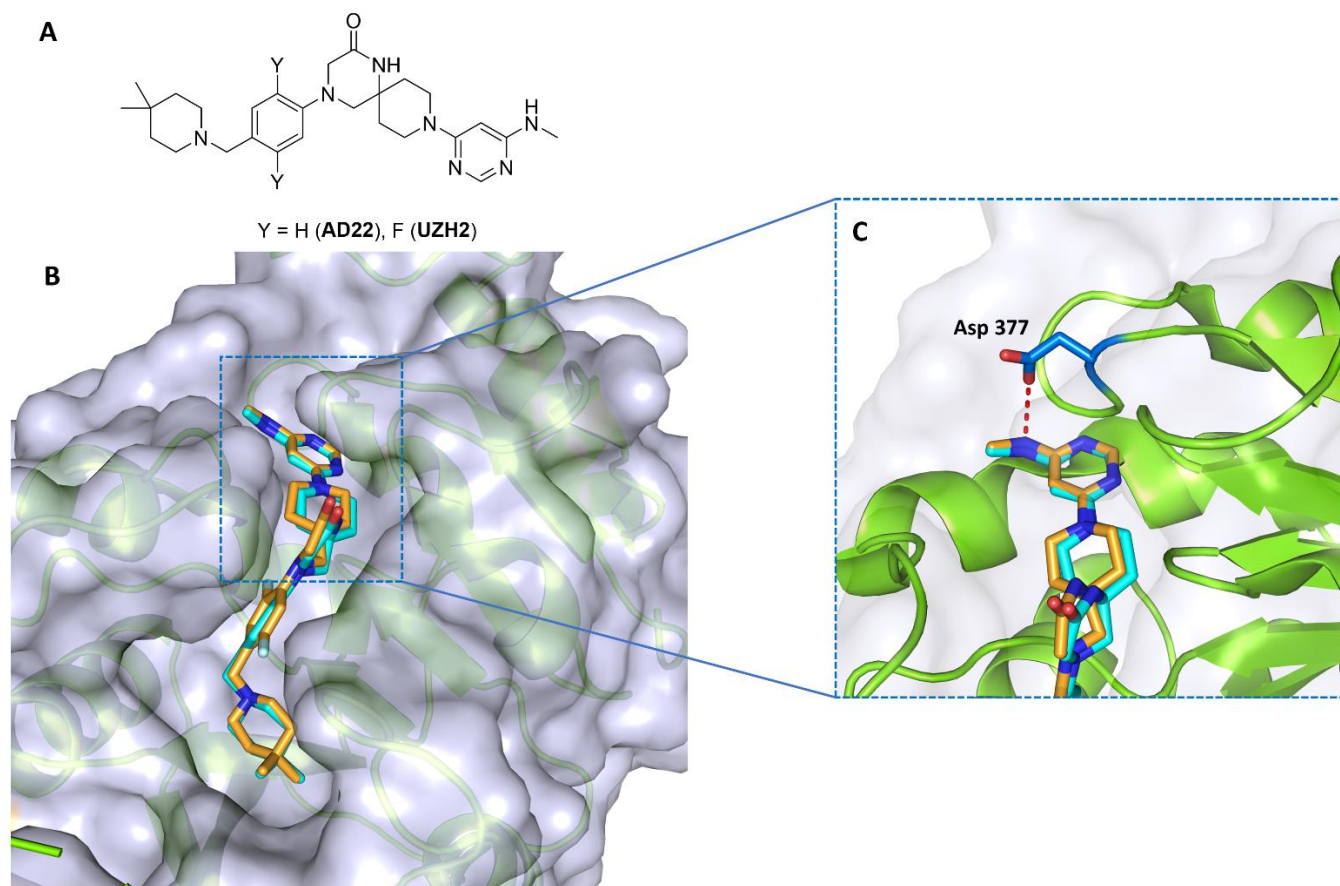


Figure 1. a) 2D structures of UZH2 and its desfluoro precursor AD22. b) Overlap of the crystal structures of METTL3 bound to AD22 (carbon atoms in cyan, PDB 7O0P) and UZH2 (carbon atoms in orange, PDB 7O2F). c) Zoom in on the hydrogen bond between the side chain of Asp377 and the methylamine of AD22 and UZH2.

Optimization of cell permeability and POI affinity

To address the low permeability, we synthesized a second set of AD22-based PROTACs (compounds 5-9), aiming to increase the lipophilicity of the molecules. The PEG linker was replaced by an alkyl chain.⁴⁶⁻⁴⁸ The positive effect of the increased lipophilicity on the cell membrane permeation was confirmed through CETSA experiments, as indicated by more pronounced stabilization effects (Figure 2). To improve the stability of the ternary complex, we decided to

change the POI ligand by replacing AD22 with the ~20-fold more potent inhibitor UZH2. As expected, the resulting PROTACs (compounds 10-13) showed a much higher affinity for METTL3-14 in comparison to their AD22 analogues (Table 1). Furthermore, the EC_{max} measured in the TCFA was substantially improved. Compounds 10, 11 and 12 showed an EC_{max} below 1 μM , with a 3- to 6-fold improvement compared to the non-fluorinated analogues (Table 1). Despite the increased cellular permeability and binding affinity to the target protein, none of the tested compounds showed degradation of METTL3-14, as measured by

Western blot at 0.2, 2 and 20 μM PROTAC concentration at multiple time points (6, 16, 36h). As the PROTACs synthesized so far featured the same handle motif (propyl diamine), we questioned its impact on the ternary complex formation and protein degradation. From previous studies, we knew that the replacement of the methyl amino group in UZH2 with an aryl or aliphatic ring can provide favorable lipophilic interaction with the edge of the METTL3-14 binding site.²⁸ Moreover, a rigid and bulky feature in the handle or the linker could lead to a PROTAC conformation more prone to cell permeation and/or ternary complex formation.^{38,49–51} With this in mind, we moved on with the synthesis of PROTACs bearing a more rigid handle/linker.

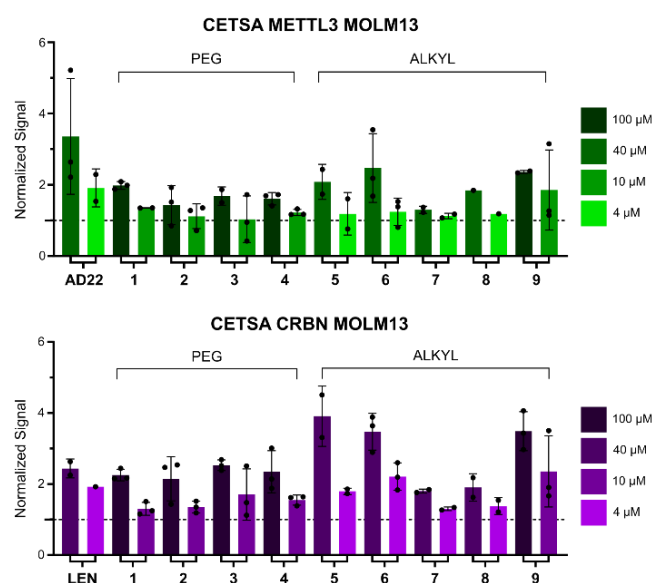


Figure 2. Evaluation of AD22-based PROTACs 1-9 in the MOLM-13 (AML) cell line. The stabilization of METTL3 (top) and Cereblon (CRBN, bottom) was quantified by CETSA at 54°C. The SAM-competitive inhibitor AD22 was employed as a control for METTL3 (top, left) while lenalidomide (LEN) was used as a control for Cereblon (bottom, left).

Optimization of length and rigidity of the linker

The next set of seven PROTAC molecules contained a benzyl diamine handle instead of propyl diamine. In addition, we varied the length of the linear portion of the linker. We retained the alkyl (compounds 14-17) and alkyl-triazole linker (compounds 18-20) from previous optimization steps. The presence of the aromatic ring significantly improved the affinity for METTL3-14 (measured by the FRET-based binary assay) as well as the values of EC_{max} (Table 1). Substantial degradation of both METTL3 and METTL14 proteins after 24-hours incubations was observed with 2 μM PROTAC concentration in MOLM-13 cells. Compounds 14, 19 and 20 reduced the level of both METTL3 and METTL14 by 52%, 33% and 42%, respectively. The most promising derivative, PROTAC 14, contained a shorter linker in comparison with the other PROTACs of this set. Furthermore, we synthesized another set of 11 PROTACs that contained lipophilic and rigid handles (piperidine, piperazine, triazole) in combination with different alkyl linker lengths. After a round of protein degradation screening in cells and quantification by Western blot analysis (2 μM , 24h MOLM-13), the compounds featuring piperidine

(compounds 21-25) or piperazine (compounds 29-32) handles exhibited the highest degradation efficacy (Table 1, Figure 3A).^{52,53} The correlated degradation of the two proteins of the heterodimeric complex METTL3-14 provides evidence that a PROTAC binding at the SAM-pocket of METTL3 is able to degrade both proteins (Figure 3B, S1). PROTAC 30 displayed the most significant degradation activity, achieving a reduction of both METTL3 and METTL14 of about 60%. In contrast, the PROTACs with a triazole ring as a handle (compounds 26 and 27) performed worse, showing a degradation efficacy of 13% and 12% respectively.

The highest degradation (50-60%) was achieved with compounds featuring a linker length spanning between five to seven atoms, i.e., PROTACs 14, 22, 23 and 30. The TCFA shows gradual EC_{max} improvement when reducing the linker length, as we can see for the piperidine handle series PROTACs 25, 24, 23, 22 and 21 (Figure 3C). Among them, the shortest PROTAC, compound 21, has the best EC_{max} (0.06 μM), but in terms of degradation, it is worse than its slightly longer analogues 22 and 24, with 21%, 46% and 36% METTL3 reduction, respectively. A possible explanation of the discrepancy between the biochemical TCFA and the cellular degradation assay is that the TCFA employs truncated protein constructs. PROTAC 21 might be too short to form a stable ternary complex with full-length proteins, and some steric clashes can cause a non-optimal conformation of the ternary complex. This EC_{max} improvement tendency is not observed at even shorter linker lengths, as shown with PROTAC 32 (no linker) which is inactive in both TCFA and cell degradation assay. Thus, there seems to be an optimal range for the linker length (three to five methylene groups).

To further increase the rigidity of the handle/linker part, we synthesized three PROTACs (compounds 33-35) with reduced linker flexibility. Among them, PROTAC 33 turned out to be the best, showing 44% METTL3 reduction, while compounds 34 and 35 displayed a METTL3 reduction of 11% and 25% respectively. Considering that compounds 34 and 35 contain a much shorter linker than PROTAC 33, these results further highlight the importance of linker length.

Once the most promising handles and ideal length to achieve protein degradation were defined, we tried to modify the connection to the CRBN ligand.^{54,55} PROTAC 23 is linked to thalidomide at position 5. This modification is well tolerated, and the compound causes a 50% degradation of METTL3. Nonetheless, compared to its 4-substituted analogue (PROTAC 22) the difference in both degradation (50% vs 46%) and EC_{max} (0.16 μM vs 0.19 μM) is negligible (Figure 3C).

The degradation activity of selected compounds (14, 20, 22, 24, 30) was investigated in different AML cell lines (THP-1, NOMO-1 and KASUMI-1) (Figure 3A, S1). While the degradation levels observed in THP-1 and NOMO-1 cell lines were comparable to those in MOLM-13, a higher degradation of both METTL3 and METTL14 was measured in KASUMI-1. The treatment of KASUMI-1 cells with 2 μM of PROTAC 30 for 24h caused a 70% degradation of the POI.

To further validate the top PROTACs we tested some of them against cell lines of solid tumors. We decided to focus on two prostate cancer cell lines (DU145 and PC3) because

of recent evidence for the importance of METTL3 in prostate cancer.^{56,57} The selected PROTACs 14, 20, 22, 24 and 30 showed only a minor effect in the DU145 cell line. In contrast, the METTL3 levels were reduced substantially in PC3, with PROTACs 20 and 24 showing the highest degradation with 48% and 64% reduction of METTL3 (after 24 hours), respectively. This result indicates that the degradation activity of our PROTAC molecules is not limited to leukemia

cell lines, but they have a good potential also against prostate cancer. Moreover, the correlated degradation of METTL3 and METTL14 was observed not only in MOLM-13 (Figure 3B) but also in all the other cell lines tested (Figure 3A, S1).

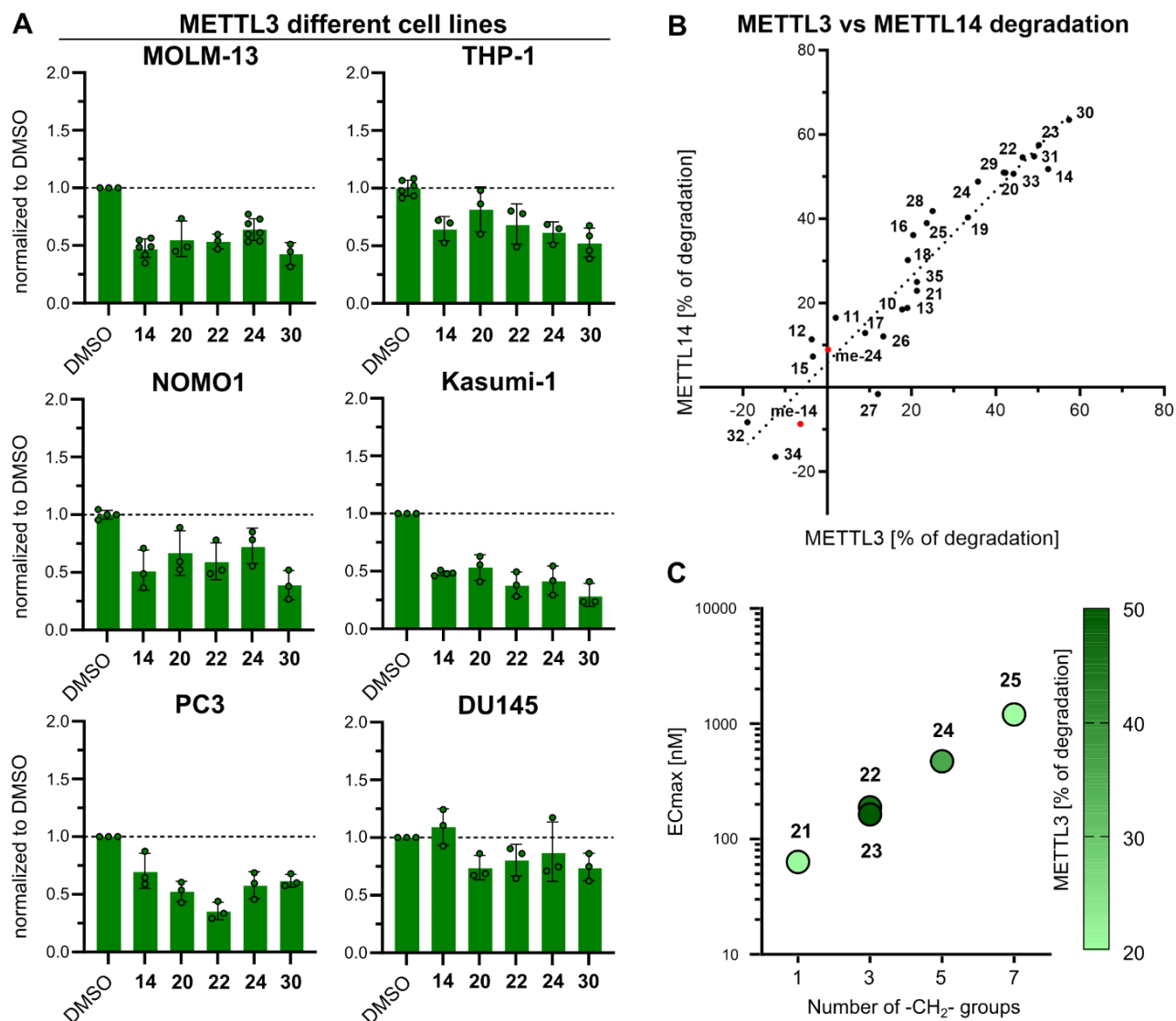
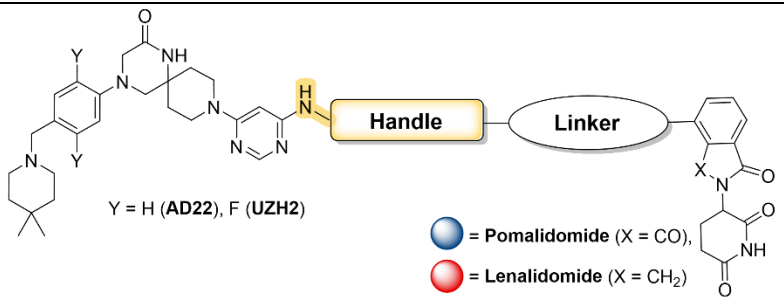
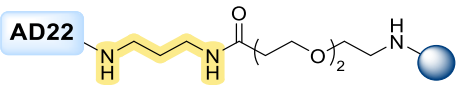
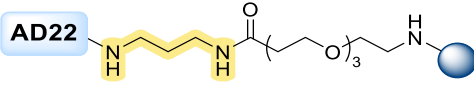
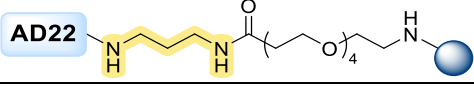
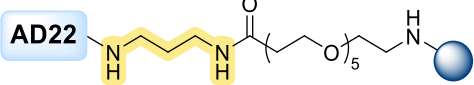
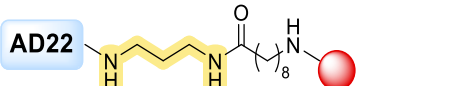
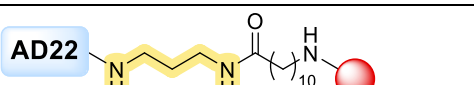
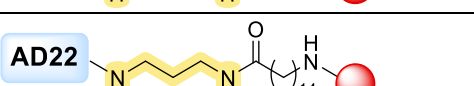
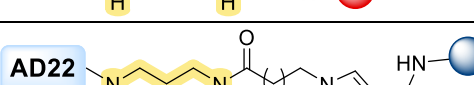
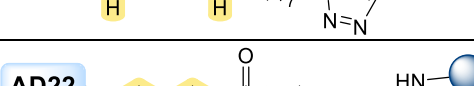
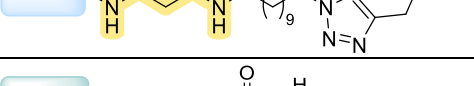
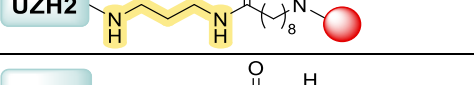
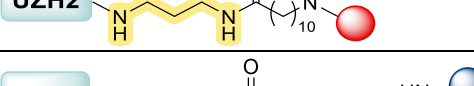
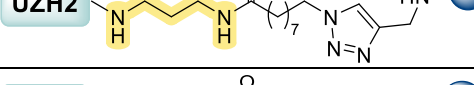
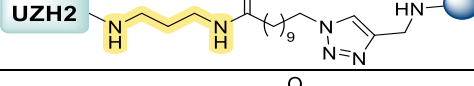
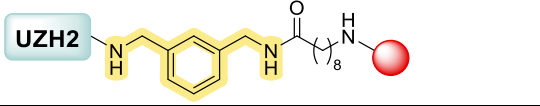
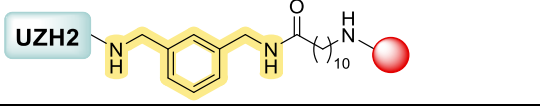
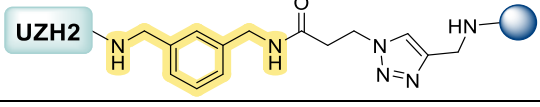
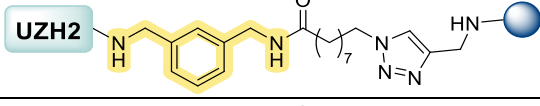
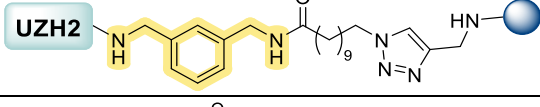
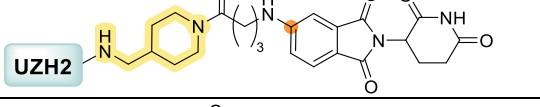
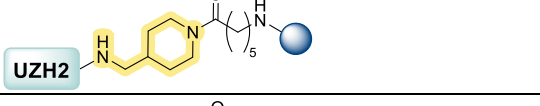
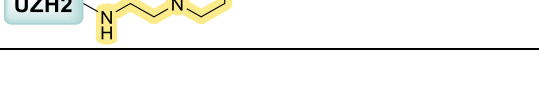


Figure 3. a) METTL3 Western blot quantification by densitometry from a cellular degradation assay with PROTAC compounds 14, 20, 22, 24 and 30 in the AML cell lines MOLM-13, THP-1, NOMO-1, KASUMI-1 and in the prostate cancer cell lines PC3, DU145. b) Correlation of the degradation of METTL3 and METTL14 in MOLM-13 (corr. coeff. of 0.95). c) Correlation between the number of -CH₂- groups in the linker and the EC_{max} value measured in the TCFA. The color of the data points reflects the degradation of METTL3 as measured by Western blot in MOLM-13 (legend on the right). While the EC_{max} improves until the shortest length of the linker (one -CH₂-), the highest degradation is observed at intermediate lengths, i.e., (-CH₂)₃.

Table 1. Synthesized PROTACs and activity data.

Entry	Structure	MOLM-13 West. blot at 24h 2 μ M comp conc. Degradation (%) of METTL3 and METTL14	EC _{max} (nM) \pm SD	IC ₅₀ (nM) \pm SD
 <p>Y = H (AD22), F (UZH2)</p> <p>● = Pomalidomide (X = CO), ● = Lenalidomide (X = CH₂)</p>				
1		/ /	6800 (n = 1)	2470 \pm 790
2		/ /	2800 \pm 280	1060 \pm 220
3		/ /	1900 (n = 1)	590 \pm 130
4		/ /	2000 (n = 1)	640 \pm 120
5		/ /	660 \pm 20	260 \pm 30
6		/ /	3600 (n = 1)	520 \pm 60
7		/ /	5300 (n = 1)	1220 \pm 90
8		/ /	2200 (n = 1)	480 \pm 100
9		/ /	6700 (n = 1)	1800 \pm 290
10		18 \pm 6 18 \pm 16	200 \pm 110	66 \pm 10
11		< 10 17 \pm 22	910 \pm 40	300 \pm 40
12		/ 11 \pm 27	320 \pm 160	67 \pm 21
13		19 \pm 20 19 \pm 13	1800 \pm 250	220 \pm 40
14		52 \pm 8 52 \pm 6	250 \pm 0	11 \pm 1

15		/	< 10	640 ± 30	33 ± 4
16		24 ± 14	39 ± 13	430 ± 180	67 ± 11
17		< 10	13 ± 6	920 ± 160	160 ± 20
18		19 ± 13	30 ± 12	80 ± 0	14 ± 3
19		33 ± 17	40 ± 16	920 ± 150	88 ± 21
20		42 ± 13	51 ± 10	860 ± 240	200 ± 30
21		21 ± 9	23 ± 9	60 ± 30	n.d.
22		46 ± 6	55 ± 11	190 ± 90	11 ± 1
23		50 ± 12	57 ± 8	160 ± 80	33 ± 12
24		36 ± 9	50 ± 13	470 ± 80	58 ± 12
25		20 ± 9	36 ± 7	1200 ± 120	110 ± 10
26		13 ± 30	12 ± 5	190 ± 80	34 ± 11
27		12 ± 43	/	1100 ± 330	610 ± 230
28		25 ± 3	42 ± 7	5100 (n = 1)	370 ± 60
29		42 ± 14	51 ± 11	80 ± 0	n.d.
30		57 ± 10	63 ± 18	70 ± 30	27 ± 6

31		49 ± 33	55 ± 24	110 ± 40	n.d.
32		/	/	/	n.d.
33		44 ± 6	51 ± 19	70 ± 10	n.d.
34		/	/	120 ± 30	n.d.
35		21 ± 11	25 ± 3	20 ± 0	n.d.

Validation of PROTACs cellular activity

Next, we treated MOLM-13 cells with PROTACs 14 and 30 at five different concentrations (Figure 4). As expected, the concentration dependence shows the so-called Hook effect,^{58,59} resulting from a saturation of CRBN and METTL3-14 at high PROTAC concentrations, where the PROTAC/CRBN and PROTAC/METTL3-14 binary complexes prevent the ternary complex formation and thus degradation. This result confirms that our compounds behave according to the principle of the PROTAC mechanism of action. For PROTAC 30, the highest degradation was observed at 0.1 μM concentration, reaching up to 60% degradation, and for PROTAC 14 the highest effect was seen at 1 μM , with a METTL3 reduction of around 50%.

Furthermore, we evaluated the METTL3-14 protein levels after PROTAC treatment in combination with high concentrations of the small-molecule inhibitors lenalidomide or UZH2 (Figure 5A). These controls consist of saturating the binding pockets of CRBN or METTL3-14, respectively, thus preventing the formation of the ternary complex. Cells were treated with PROTACs 20 and 24 under three different conditions: 2 μM PROTAC, 2 μM PROTAC + 10 μM lenalidomide, 2 μM PROTAC + 10 μM UZH2. As expected, we did not observe any degradation when applying a high concentration of lenalidomide. Interestingly, the presence of a high UZH2 concentration led to elevated levels of METTL3-14 both in the control as well as in combination with the PROTAC. This observation indicates a possible cellular compensatory mechanism aimed at preserving the protein catalytic activity in the presence of an inhibitor.⁶⁰ It also offers a potential explanation for the difficulties in reaching degradation levels of METTL3-14 above 50%.

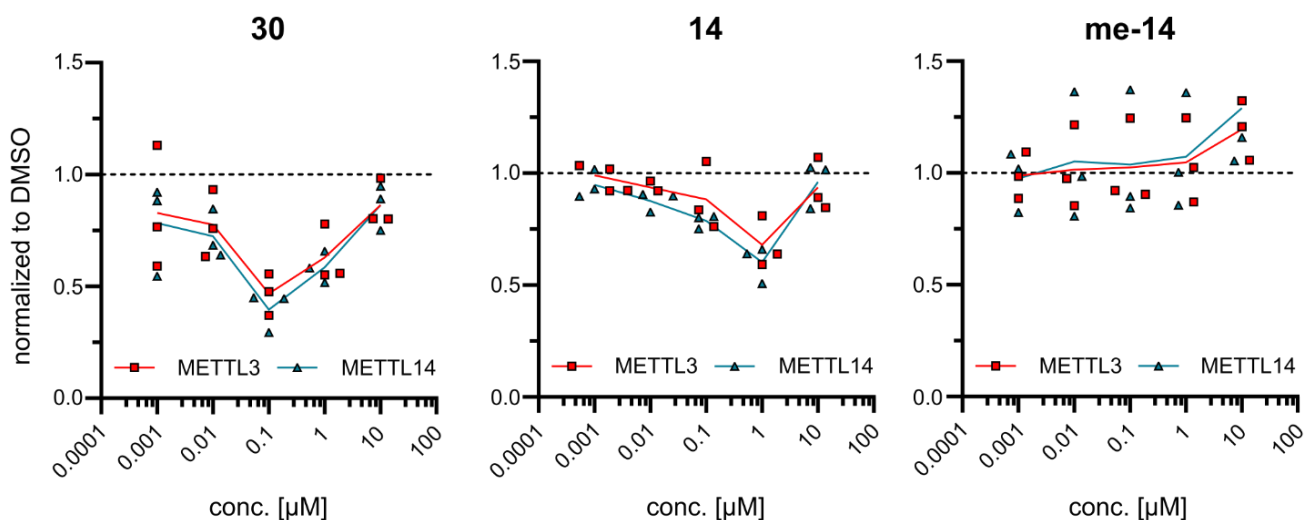


Figure 4. Concentration dependence of METTL3 (red) and METTL14 (blue) degradation by PROTACs 30, 14 and the methylated negative control of 14 (**me-14**) in MOLM-13 cells (see Figure S2 for representative Western blot).

To confirm that our compounds lead to protein degradation by hijacking the Ubiquitin-proteasome system (UPS), we synthesized negative controls based on a single methylation, which results in inactive lenalidomide/pomalidomide derivatives.⁶¹⁻⁶³ Thus, we prepared the methylated versions of PROTACs 14 and 24 (me-14 and me-24) (Figure 5B). These methylated compounds did not show any METTL3-14 degradation at standard testing conditions (2 μ M, 24h) (Figure 5C). Furthermore, compound me-14 was tested in a concentration-dependent manner, showing no degradation and even increasing METTL3 levels at 10 μ M (Figure 4), similar to the UZH2 inhibitor alone. Both control PROTACs gave no signal in the biochemical ternary complex formation assay (Figure 5D). The methylated derivatives are inactive, indicating their inability to form a ternary complex and further confirming the specificity of our PROTACs. Compound me-14 was also tested in CETSA on both METTL3 and CRBN to provide evidence that it is cell permeable and engages the POI and not CRBN (i.e., validation of the negative control). As expected, the compound showed stabilization of METTL3 but not of CRBN (Figure S3).

Lastly, we set up an *in vitro* ubiquitination assay to quantify the ubiquitination of METTL3 and METTL14 in the presence of different concentrations of PROTACs. Compounds 14 and me-14 were tested at 2 μ M, 8 μ M and 32 μ M (Figure 5E). While me-14 does not increase the ubiquitination of METTL3 compared to the control without compound, compound 14 raises the ubiquitination level of METTL3 to ~40% at 2 μ M. The decrease of ubiquitination at higher concentrations of compound 14 is consistent with the Hook effect. The ubiquitination of METTL14 is not as pronounced (Figure S4). This can indicate that the ubiquitination site(s) is (are) mainly on METTL3. Interestingly, Zeng et al. showed that METTL14 can get ubiquitinated by STUB1 in the METTL3-14 interface and METTL3 therefore seems to prevent METTL14 ubiquitination.⁶⁴ The simultaneous degradation of METTL3 and METTL14 caused by the PROTACs (Figure 3B) could be explained by either both proteins being subjected to the proteasome as a complex or by the reduced stability of METTL14 without METTL3.

Overall, among the 35 PROTAC compounds synthesized in this study, five showed significant activity in different cell lines (AML and prostate cancer) with METTL3-14 degradation up to 70% of endogenous level (Figure 3A). The concentration-dependent degradation activity (Hook effect, Figure 4), correlation in the degradation of the two proteins of the METTL3-14 heterodimeric complex (Figure 3B), methylated PROTAC controls (Figure 5), and the additional validation experiments with competitive small-molecule ligands (Figure 5A), provide strong evidence of cellular target engagement and selectivity of our PROTACs.

To assess whether degradation induced by our compounds translated into enhanced cell death, we performed cell viability assays (Figure 6A). Significant effects on cell viability of some PROTACs were observed only at the highest concentration tested (10 μ M), but not at concentrations previously considered optimal for METTL3-14 degradation. Interestingly, on PC3 cell line only PROTACs (compounds 22, 24 and 30) and not UZH2 showed antiproliferative effect.

To better understand cell viability results in MOLM-13 cell line, we measured the changes in cellular m⁶A/A levels (by LC-MS quantification) after PROTAC treatment (Figure 6B). At 2 μ M (concentration used for degradation screening) we did not observe significant effects on the levels of m⁶A/A (except for a slight reduction for compound 22). Measurable reduction of m⁶A/A was observed at 10 μ M concentration. Taking into consideration the concentration-dependent activity of PROTAC molecules (Hook effect), it is more likely that the observed reduction in m⁶A modification is due to the inhibition of the catalytic activity of METTL3 by the UZH2-based warhead rather than protein degradation. Partial inhibition of the catalytic activity might also explain the observed cytotoxic effect at the highest tested concentrations of PROTACs. In conclusion, the modest cytotoxicity and reduction of m⁶A/A suggest that degradation levels higher than 50-70% are required to observe phenotypic effects specific to PROTAC-induced METTL3-14 degradation.

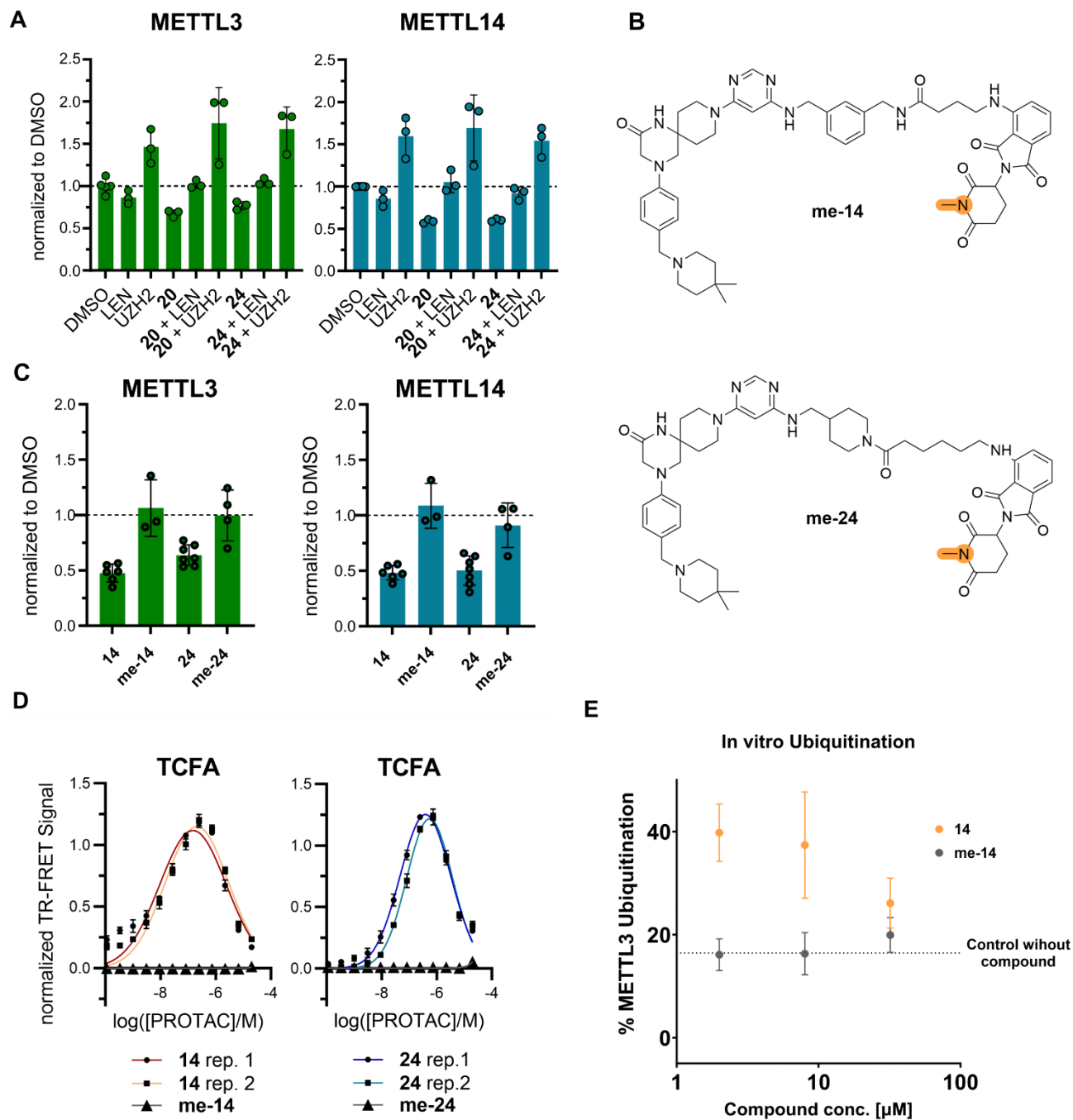


Figure 5. a) Evaluation of METTL3 and METTL14 level in presence of lenalidomide or UZH2 in MOLM-13. b) Chemical structures of PROTAC negative controls **me-14** and **me-24**. c) METTL3 (left) and METTL14 (right) Western blot quantification by densitometry of PROTACs **14** and **24** in comparison with their negative controls **me-14** and **me-24** in MOLM-13. d) Biochemical FRET-based ternary complex formation assay (TCFA) with PROTACs **14** and **24** and their methylated negative controls **me-14** and **me-24**. e) In vitro ubiquitination assay results with compound **14** and its negative control **me-14**. All data originate from biological/biochemical duplicates or more (see Figure S4 for representative Western blot).

Conclusions

Here, we report a medicinal chemistry design of PROTACs against the m⁶A-RNA writer METTL3-14. We used as starting information the crystal structure of METTL3-14 in complex with the potent (IC₅₀ = 5 nM) and selective inhibitor UZH2. We efficiently optimized the PROTAC linker by first employing the desfluoro derivative of UZH2 as moiety for METTL3-14. While PEG- and alkyl-based linkers were considered initially, only the PROTACs with alkyl-based linkers demonstrated cell penetration. Subsequently, we synthesized 26 PROTACs based on UZH2 with alkylic linkers of varying lengths. The formation of the ternary complex and

ubiquitination of METTL3 were confirmed by a FRET-based assay and an *in vitro* ubiquitination assay. Notably, three PROTACs with distinct rigid extensions of UZH2 achieved substantial METTL3 degradation (50% or higher) in multiple AML cell lines and the prostate cancer cell line PC3, showcasing their potential as valuable tools in targeted protein degradation research. In comparison with the catalytic inhibitor UZH2, the PROTACs 22, 24, and 30 show higher antiproliferative activity on the prostate cancer PC3 but not on AML cell lines. The elevated level of METTL3-14 in the presence of UZH2 and lack of reduction of the m⁶A/A level of polyadenylated RNA (measured by LC/MS) suggest that a substantially higher degradation of METTL3-14 (probably above 90%) is required for a strong antiproliferative effect.

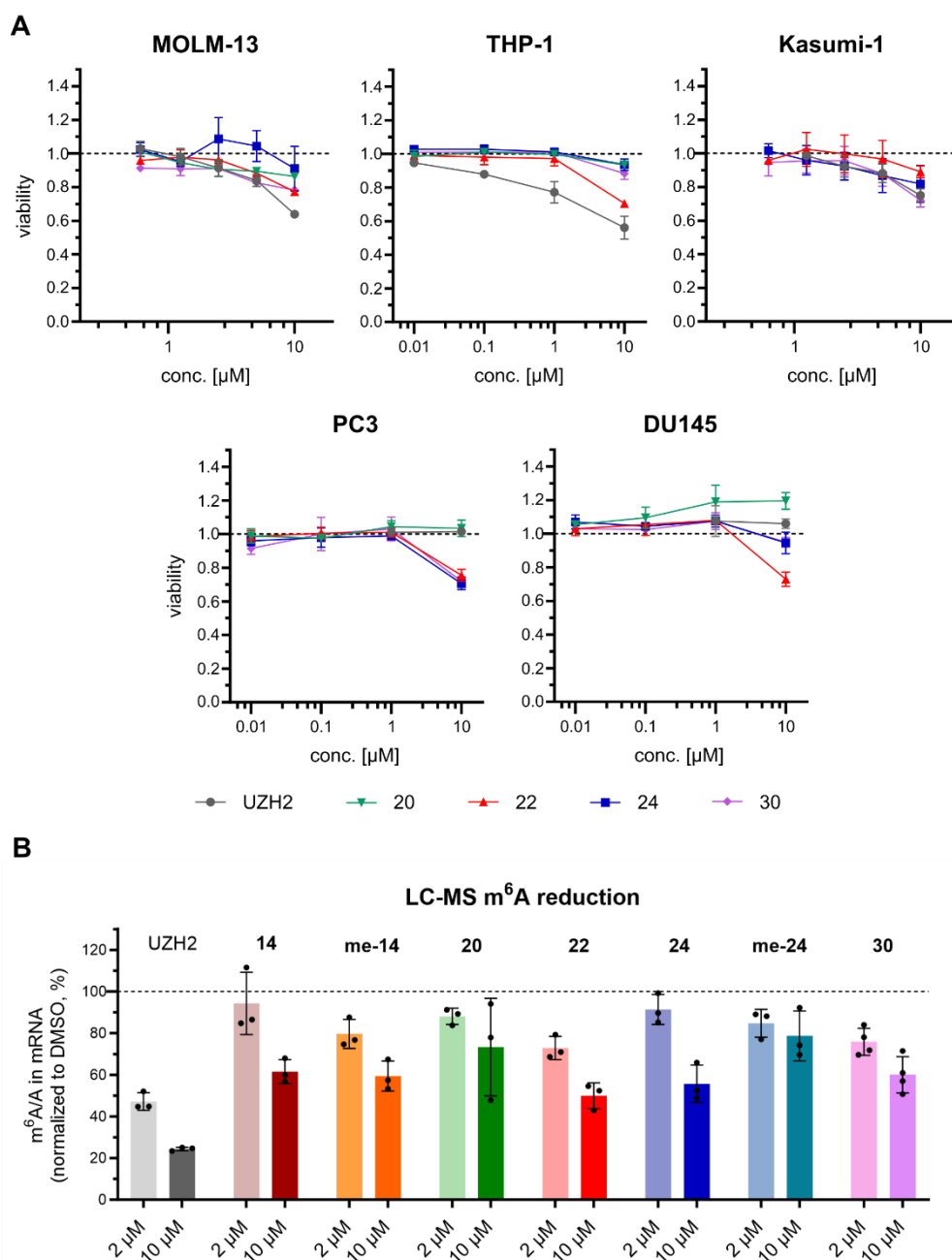
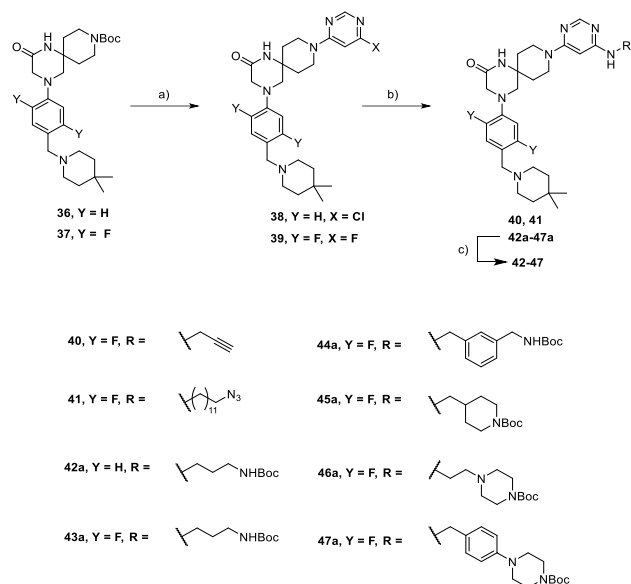


Figure 6. a) Cell viability assay for PROTACs **20**, **22**, **24**, **30** and the METTL3 catalytic inhibitor **UZH2** in AML cell lines (top) and prostate cancer cell lines (bottom). b) LC-MS quantification of m⁶A/A levels in polyadenylated RNA in MOLM-13.

Synthesis

Starting from the spiro compounds **36** and **37**, the preparation of POI ligands bearing the handle moiety was conducted following the general strategy reported in Scheme 2:

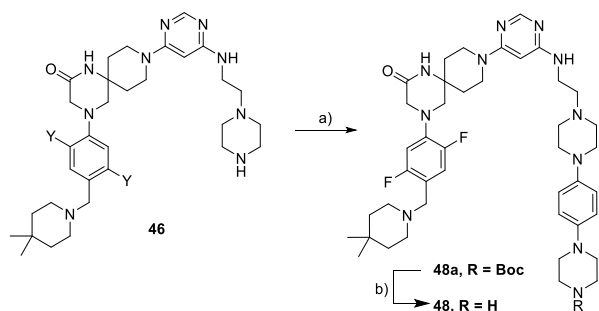
Scheme 2. Synthesis Route for Compounds 40-47^a



^aReagents and conditions: (a) (i) HCl aq. 37 %, MeOH; (ii) for **38** and **39**: 4,6-dichloro pyrimidine (**38**)/4,6-difluoro pyrimidine (**39**), TEA, iPrOH; (b) RNH₂, TEA, DMSO (**40**, **41**)/EtOH (**42a-47a**); (c) for **42-47**: TFA, DCM.

After Boc deprotection followed by an S_NAr reaction with 4,6-dichloro or difluoro pyrimidine, compounds **38** and **39** were obtained. A second S_NAr was needed to afford compounds **40**, **41**, **42a-47a**. Interestingly, due to the poor reactivity of chloro-pyrimidine **38** towards S_NAr, we were only able to prepare compounds **42a** and **43a**. Switching to its fluorinated analogue **39** was necessary to synthesize compounds **40**, **41**, **44a-47a** in good yield (from 50 to 70 %). Compounds **42-47** were then obtained upon removal of the protecting group from the precursors **42a-47a**.

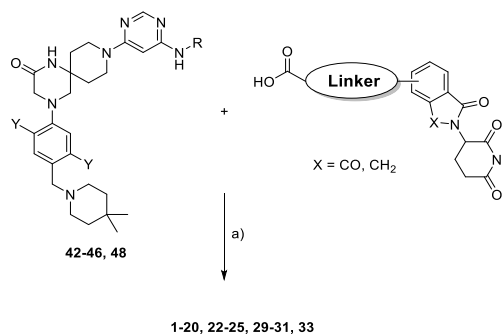
Scheme 3. Synthesis Route for Compound 48^a



^aReagents and conditions: (a) tert-butyl 4-(5-bromopyrimidin-2-yl) piperazine-1-carboxylate, CuI, (L)-proline, K₂CO₃, DMSO; (b) HCl 4M in dioxane, MeOH.

Through a Ullmann-type reaction, we combined compound **46** with Boc-protected 4-(5-bromopyrimidin-2-yl) piperazine.⁶⁵ The desired intermediate **48a** was obtained in low yield and upon Boc deprotection afforded compound **48** (Scheme 3).

Scheme 4. Synthesis Route for Compounds 1-20, 22-25, 29-31, 33^a

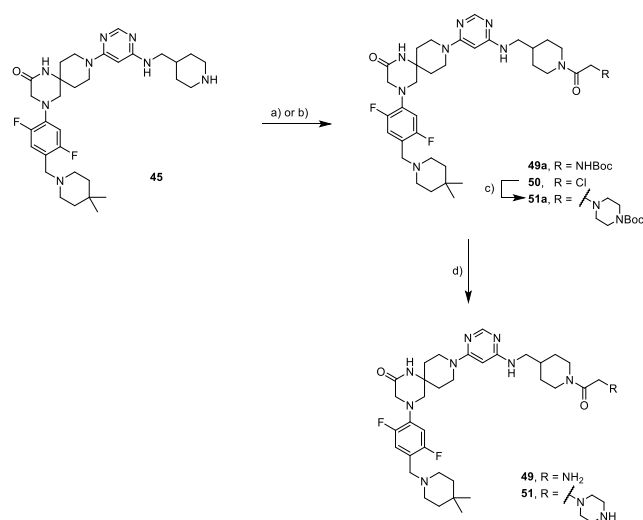


^aReagents and conditions: (a) HATU (**1-4**, **8**, **9**, **29-31**)/COMU (**5-7**, **10-28**, **32-35**), DIPEA, DMF.

Compounds **1-20**, **22-25**, **29-31**, and **33** were synthesized via an amide coupling reaction between compounds **42-46**, **48** and the corresponding pomalidomide/lenalidomide carboxylic acids. HATU coupling agent provided decent yields only for compounds **1-4**, **8**, **9** and **29-31**. For the other molecules, COMU performed better and provided the desired products with yields up to 60% (Scheme 4).

The final amide coupling (Scheme 4) did not work out for compounds **21** and **35**. Therefore, the synthetic route was slightly modified. Both intermediate **49** and **51** were prepared starting from **45**. An amide coupling between the latter and Boc-glycine, followed by amino group deprotection, yielded compound **49**. For the synthesis of compound **51**, acetylation of **43** using 2-chloroacetyl chloride resulted in the formation of **50**. Afterwards, we converted **50** into **51** through an S_N2 reaction with Boc-piperazine, followed by the removal of the protecting group (Scheme 5).

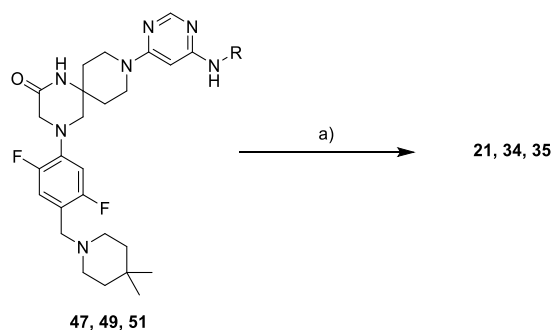
Scheme 5. Synthesis Route for Compounds 49, 51^a



^aReagents and conditions: (a) For **49a**: Boc-glycine, COMU, DIPEA, DMF; (b) for **50**: 2-chloroacetyl chloride, DIPEA, dry THF; (c) for **51a**: Boc-piperazine, DMSO, 50°C; (d) for **49** and **51**: TFA, DCM.

With intermediate **49** and **51** in our hands, we were finally able to obtain PROTACs **21** and **35** using S_NAr and 4-fluoro thalidomide. Using the same reaction as the final step, we prepared PROTAC **34** from compound **47** (Scheme 6).

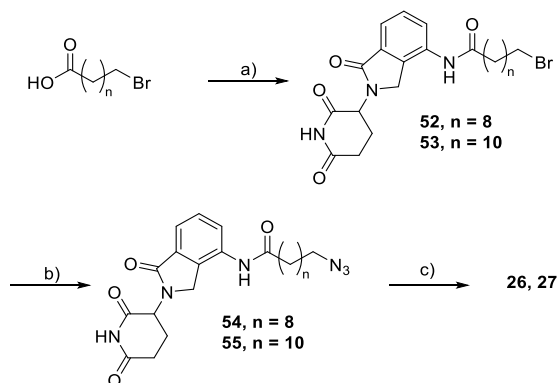
Scheme 6. Synthesis Route for Compounds 21, 34, 35^a



^aReagents and conditions: (a) For **21**, **34** and **35**: 4-fluoro thalidomide, TEA, DMSO.

To synthesize **26** and **27**, compounds **52** and **53** were first prepared starting with lenalidomide, which was reacted with the corresponding carboxylic acids.⁶⁶ A following S_N2 reaction with NaN₃ allowed us to prepare intermediates **54** and **55**.⁶⁷ PROTACs **26** and **27** were finally obtained through the Click reaction (Scheme 7).

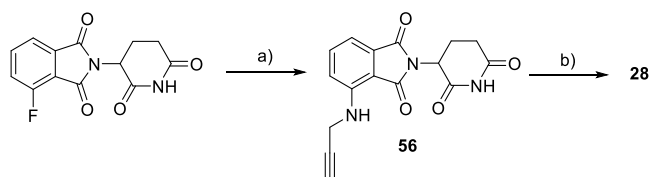
Scheme 7. Synthesis Route for Compounds 26, 27^a



^aReagents and conditions: (a) (i) SOCl₂; (ii) lenalidomide, THF; (b) NaN₃, DMF; (c) **40**, CuSO₄, Na ascorbate, THF.

Compound **56** was obtained from a S_NAr reaction between 4-fluoro thalidomide and propargyl amine.⁶⁸ Similarly to **26** and **27** (Scheme 7), the Click reaction between **56** and **41** was employed to synthesize PROTAC **28** (Scheme 8).

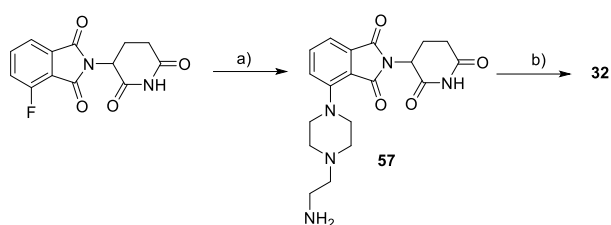
Scheme 8. Synthesis Route for Compound 28^a



^aReagents and conditions: (a) propargyl amine, TEA, DMSO; (b) **41**, CuSO₄, Na ascorbate, THF.

Following the same procedure used for **56** (Scheme 8), we prepared the protected version of intermediate **57**. After Boc removal, PROTAC **32** was obtained via S_NAr reaction between compounds **57** and **39** (Scheme 9).

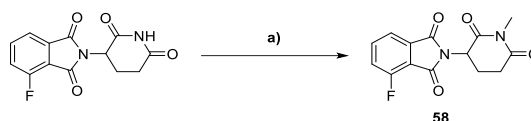
Scheme 9. Synthesis Route for Compound 32^a



^aReagents and conditions: (a) (i) tert-butyl (2-(piperazin-1-yl) ethyl) carbamate, DIPEA; DMSO; (ii) HCl 4M in dioxane, MeOH; b) **39**, DIPEA, DMSO.

For the synthesis of **me-14** and **me-24** (Scheme 10), 4-fluoro thalidomide was methylated using CH₃I.⁶⁹ The two PROTACs were then synthesized from **58**, following the synthetic route used for the non-methylated analogues PROTACs **14** and **24** (Scheme 4).

Scheme 10. Synthesis Route for Compound 58^a



^aReagents and conditions: (a) CH₃I, K₂CO₃, DMF.

Material and methods

METTL3-14 expression and purification

For determining the half maximal inhibitory concentration (IC₅₀) with the full-length complex, the recombinant complex construct pFastBacDual-StrepII-GFP-TEV-METTL3-His-TEV-METTL14 was expressed using the baculovirus/Sf9 insect cell expression system and purified as described previously.²¹

For ternary complex formation assays, genes containing the methyltransferase domains (MTD) of METTL3 (residues 354–580) and METTL14 (residues 107–395) were cloned into the MacroBac vector 438-GST.⁷⁰ A histidine tag (His) was inserted at the N-terminus of GST by site-directed mutagenesis to yield the construct 438-His-GST-METTL3^{MTD}-METTL14^{MTD}. Recombinant baculovirus to express the complex of His-GST-METTL3^{MTD} and METTL14^{MTD} was generated using the Bac-to-Bac system. For protein expression, suspension cultures of Sf9 cells in Sf-90 II SFM medium (Thermo Fisher) were infected at a density of 2×10⁶ ml⁻¹. Cells were harvested 72 hours post-infection, resuspended in Buffer A (50 mM Tris-HCl pH 8.0, 500 mM NaCl) supplemented with Protease Inhibitor Cocktail (Roche Diagnostics GmbH, Germany), phenylmethylsulfonyl fluoride (PMSF), Salt Active Nuclease (Merck), and lysed by sonication. The protein complex was purified by Ni-affinity chromatography on a 5 mL HisTrap HP column (Cytiva) equilibrated and washed with Buffer A and eluted with 250 mM imidazole. The complex was further purified by size exclusion chromatography using a Superdex 200 Increase 10/300 GL column (Cytiva) in 20 mM Tris-Cl, pH 8.0, and 200 mM KCl.

The complex was aliquoted flash-frozen in liquid nitrogen and stored at -80 °C until further use.

Reader-based TR-FRET assay

The inhibitory potencies of the PROTACs for METTL3 were quantified by a homogeneous time-resolved fluorescence (HTRF)-based enzyme assay as previously described.³⁷ Briefly, the level of m⁶A in an RNA substrate after the reaction catalysed by METTL3-14 was quantified by measuring specific binding to the m⁶A reader domain of YTHDC1 (residues 345-509) by HTRF. PROTACs that inhibit METTL3 decrease the m⁶A level and thus reduce the HTRF signal. Dose-response curves of titrations with the PROTACs were plotted in OriginLab 2018 and fitted with nonlinear regression “log(inhibitor) vs. normalized response with variable slope” from which IC₅₀ values were determined. Each PROTAC was measured in triplicates on a Corning 384 U Bottom White Polystyrene plate.

Biotinylated CRBNTBD expression and purification

His-TEV-CRBN^{TBD}-Avi was created by inserting a tobacco etch virus (TEV) cleavage site at the N-terminus and an Avi-tag at the C-terminus of CRBN thalidomide binding domain (TBD, CRBN residues 318-442) and the construct was cloned into pETDuet-1 vector between SacI and HindIII restriction sites together with full-length enzyme BirA which was cloned into the same vector between NdeI and XhoI restriction sites.

The construct was overexpressed in Rosetta (DE3) cells upon induction with 100 μM isopropyl thio-beta-D-galactoside (IPTG) for 20 h at 18 °C. The expression medium was supplemented with 50 μM D-biotin. Harvested cells were resuspended in lysis buffer containing 100 mM Tris-HCl, pH 8.0, 500 mM NaCl, 1 mM 1,4-dithiothreitol (DTT), 1 mM phenylmethylsulfonyl fluoride (PMSF), and 1 mM ethylenediaminetetraacetic acid (EDTA) and lysed by sonication. The lysates were centrifuged at 18,000 rpm at 4 °C for 1 h in an SS-34 rotor. The soluble fraction was then loaded onto a HisTrap FF crude column (GE Healthcare) and washed with lysis buffer supplemented with 50 mM imidazole. The protein was eluted with a buffer containing 250 mM imidazole, 100 mM Tris-HCl, pH 8.0, and 500 mM NaCl. Recombinant TEV protease cleaved the His₆ tag during overnight dialysis at 4 °C against 100 mM Tris-HCl, pH 8.0, and 500 mM NaCl buffer. The dialyzed sample was passed through the HisTrap FF crude column to remove His₆-tagged TEV protease and uncleaved protein. The protein was further purified by size-exclusion chromatography using a HiLoad 16/600 Superdex 200 pg column (GE Healthcare) in 50 mM HEPES, pH 7.5 and 150 mM NaCl buffer. The protein was aliquoted and stored at -80 °C until further use. Biotinylation was confirmed by an avidin shift assay, where a final CRBN-Avi of 5 μM was mixed with different amounts of NeutrAvidin (10, 20, 40 μM) (Thermo Fisher # 31000) and the proteins were analysed by SDS-PAGE (data not shown).

Ternary complex formation assay

Ternary complex formation between the PROTACs, METTL3, and CRBN was quantified by a homogeneous time-resolved fluorescence (HTRF)-based enzyme assay. The

HTRF signal of a titration series with PROTACs at constant METTL3 and CRBN concentrations underlies the hook effect leading to a characteristic bell-shaped curve where the concentration of the ternary complex decreases at high PROTAC concentrations. Curves of titrations with the PROTACs were plotted in GraphPad Prism 9.5.1 and fitted with a Gaussian function if appropriate. His-GST-METTL3^{MTD}-METTL14^{MTD} was used at a final concentration of 15 nM. CRBN^{TBD}-Avi(biotin) was used at a final concentration of 10 nM. XL665-conjugated streptavidin (Cisbio, 610SAXLB) was used at a final concentration of 1.25 nM. Anti-GST Eu³⁺-labelled antibody (Cisbio, 61GSTKLB) was used at a final concentration of 0.8 nM. The final reaction volume was 20 μL in 50 mM HEPES (pH 7.5), 150 mM NaCl, 0.1 % BSA, 100 mM KF. The assays were carried out in triplicate on a Corning 384 U Bottom White Polystyrene plate (20 ul working volume). The reaction was incubated for at least 3 hours at room temperature (RT) in the dark before the HTRF signal was measured using a Tecan Spark plate reader (Tecan). The plate reader recorded with a delay of 100 μs the emission at 620 and 665 nm after the excitation of the HTRF donor with UV light at 320 nm. The ratio of the emissions:

$$F = \frac{\text{acceptor}_{665 \text{ nm}}}{\text{donor}_{620 \text{ nm}}}$$

was considered for further analysis. The maximal control contained Compound 16, the blank contained no compounds – this was replaced by the appropriate buffer (with DMSO). The Hook curves were determined by normalization with the maximal control (compound 16) where the maximum of the Hook curve is determined as fraction of the maximum of compound 16 for each PROTAC. The concentrations resulting in the maximum signal (EC_{max}) and the amplitudes of the Hook curves were determined from the parameters of the Gaussian fit (if appropriate) or as the coordinates of the data-point with the highest TR-FRET signal.

In vitro ubiquitination assay

For the cell-free in vitro ubiquitination of METTL3-METTL14 purified E1, E2, ubiquitin, CUL4A-RBX1, Cereblon-DDB1 and METTL3-METTL14 were used. Human full-length METTL3-METTL14 was expressed and purified as described above. Human full-length cereblon-DDB1 and 6xHis-CUL4A-6xHis-RBX1 were co-expressed using the baculovirus/Sf9 insect cell expression system and purified by nickel affinity chromatography on a 5 mL HisTrap HP column (Cytiva) followed by anion exchange chromatography on a 5 mL HiTrap Q HP column (Cytiva) and a final gel-filtration step on a HiLoad 16/600 Superdex 200 pg column. Purified recombinant human UBE1 E1 (E-305-025) was purchased from R&D Systems, UbcH5a E2 (23-029) from Merck and ubiquitin (SBB-UP0013) from South Bay Bio. For the ubiquitination reaction, components were mixed to final concentrations of 0.06 μM UBE1, 1.96 μM UbcH5a, 39 μM Ubiquitin, 0.33 μM CUL4A-RBX1, 0.33 μM Cereblon-DDB1, 0.5 μM METTL3-METTL14 and different concentrations of compound 14 or me-14 (0, 2, 8, or 32 μM) in reaction buffer (50 mM Tris-HCl pH 7.6, 5 mM MgCl₂, 0.2 mM CaCl₂, 1 mM DTT, 100 mM NaCl, 0.01 % BSA, 0.01 % Triton X-100). The final reaction volume was 15 μL. After the addition of 2 mM ATP (or the equal volume of water for the control without

ATP), the reaction mixture was incubated for 2 h at 30 °C. The reaction was stopped by adding SDS-PAGE loading buffer (final concentration: 60 mM Tris, 1.5 % SDS, 10 % Glycerol, 5 % beta-mercaptoethanol, 0.02 % bromophenolblue). The samples were then subjected to Western blot analysis for METTL3, METTL14 and Ubiquitin. The signals were quantified using the Image Studio Lite software. To determine the percentage of ubiquitinated METTL3, the fraction of unmodified METTL3 was calculated by dividing the signal of the band assigned to unmodified METTL3 by the signal of the area containing both the unmodified and (poly-)ubiquitinated METTL3 and normalizing to the control without ATP. The fraction of ubiquitinated METTL3 is 1 minus the fraction of unmodified METTL3.

Cell Culture

MOLM-13, NOMO-1, THP-1, Kasumi-1, PC3, DU145 cell lines were obtained from DSMZ-German Collection of Microorganisms and Cell Cultures GmbH. Cells were cultured in RPMI 1640 medium (11875093, Thermo Fisher Scientific) containing 10 % FBS (16140071, Thermo Fisher Scientific) and 1 % penicillin-streptomycin (15140122, Thermo Fisher Scientific) in 5 % CO₂ at 37 °C in a humidified incubator, with maintained cell densities at 0.5 - 1·10⁶ cells/mL. All cell lines were tested negative for mycoplasma contamination (PCR-based assay by Microsynth, Switzerland).

Cell viability assay

Cells were seeded in white clear-bottom 96-well plates at a density of 6-20 × 10³ cells/well in 50 µL of the complete RPMI medium and treated with 50 µL of increasing concentrations of the indicated compounds dissolved in DMSO (final concentration of compounds 0.01 - 10 µM) or DMSO only as a negative control (0.01 % (v/v)) and incubated for 72 h at 37 °C with 5 % CO₂. Cell viability was determined using a CellTiter-Glo luminescent cell viability assay (Promega) based on the detection of ATP according to the manufacturer's instructions. 100 µL of the reagent was added to each well and incubated for 10 min at room temperature. The luminescence was recorded using a Tecan Infinite 3046 M1000 microplate reader from the top. Background luminescence value was obtained from wells containing the CellTiter-Glo reagent and medium without cells. The resulting data was analyzed in GraphPad Prism 9.

Cellular Thermal Shift Assay (CETSA)

1 × 10⁷ cells of MOLM-13 cells were suspended in 100 µL PBS (10010023, Thermo Fisher Scientific) containing 2× Protease Inhibitor Cocktail (11697498001, Roche), for each condition tested. Cells were incubated with compounds or DMSO control (1 % (v/v)) for 1 h at 37 °C. They were then heat treated at 54 °C in a thermoblock for 3 min, followed by cooling to room temperature (3 min). Next, samples were lysed by threefreeze-thaw cycles in liquid nitrogen and centrifuge at 16000 g for 30 min, 4 °C. Equal volumes of control and tested samples (12 µL) were analysed by Western blot. The changes in the amount of METTL3 protein (after normalization for β-actin and/or GAPDH) were monitored by performing densitometry in Image Studio Lite software and analyzed in GraphPad Prism 9.

Cellular degradation assay

METTL3 (and METTL14) protein degradation was monitored by Western blot. Cells were treated with the indicated concentration of PROTACs or DMSO control (0.1 % (v/v)) for 24h, 37°C with 5% CO₂. Samples were then collected and lysed with RIPA buffer with added protease inhibitors (11697498001, Roche). After SDS-PAGE, proteins were transferred to a nitrocellulose membrane, blocked (with 5 % milk, 0.5 % BSA in TBST buffer) and incubated overnight with primary antibodies. The following antibodies were used: GAPDH (#2118, Cell Signaling, 1:4000), β-actin (ab8226, Abcam, 1:2000), METTL3 (ab195352, Abcam, 1:1000), METTL14 (ab220031, Abcam, 1:1000). Membranes were scanned using LI-COR Odyssey DLx Imager after incubation with appropriate secondary antibodies (anti-mouse IgG IRDye® 680RD (926-68072, LI-COR, 1:10000), Goat anti-Rabbit IgG IRDye® 800CW (926-32211, LI-COR, 1:10000)). Densitometry was performed in Image Studio Lite software and analyzed in GraphPad Prism 9.

Quantification of m6A/A ratio in polyadenylated RNA by UPLC-MS/MS analysis

UPLC-MS/MS was performed as previously described.²⁶

Briefly, MOLM-13 cells were seeded into 6 well plates at a density of 1x10⁶ cells/mL in 2 mL of complete RPMI medium. Cells were treated with the indicated concentrations of compounds or DMSO control (final concentration 0.5 % (v/v)) for 24 h. Following the incubation, cells were collected by centrifugation and washed once with PBS, and total RNA was extracted using 0.5 mL of GENEzol™ reagent according to the manufacturer's instructions. The final volume of 50 µL of total RNA eluate was subjected to two rounds of purification using 25 µL Sera-Mag magnetic oligo(dT) particles (Cytiva) per sample. The polyadenylated RNA was eluted with nuclease-free water in a final volume of 25 µL, and its concentration was determined using NanoDrop. One hundred nanograms of mRNA were digested to nucleosides and dephosphorylated in a one-pot reaction using 0.5 µL of nucleoside digestion mix (M0649S, NEB) in 25 µL of total reaction volume for 4 hours at 37 °C. The samples were used for UPLC-MS/MS analysis without further purification steps. The data were plotted using GraphPad Prism 9.

ASSOCIATED CONTENT

Supporting Information

The Supporting Information is available free of charge at <http://pubs.acs.org>.

Supplementary figures, tables, materials, synthetic procedures, characterization data, ¹H and ¹³C NMR spectra and HPLC traces for compounds 1-35, me-14 and me-24 (PDF).

AUTHOR INFORMATION

Corresponding Authors

Amedeo Cafilisch – Department of Biochemistry, University of Zurich, Winterthurerstrasse 190, CH-8057, Zurich, Switzerland;

Email: cafilisch@bioc.uzh.ch

František Zálešák – Department of Biochemistry, University of Zurich, Winterthurerstrasse 190, CH-8057, Zurich, Switzerland;

Email: f.zalesak@bioc.uzh.ch

Authors

Francesco Errani - Department of Biochemistry, University of Zurich, Winterthurerstrasse 190, CH-8057, Zurich, Switzerland;

Annalisa Invernizzi - Department of Biochemistry, University of Zurich, Winterthurer-strasse 190, CH-8057, Zurich, Switzerland;

Marcin Herok - Department of Biochemistry, University of Zurich, Winterthurerstrasse 190, CH-8057, Zurich, Switzerland;

Elena Bochenkova - Department of Biochemistry, University of Zurich, Winterthurer-strasse 190, CH-8057, Zurich, Switzerland;

Fiona Stamm - Department of Biochemistry, University of Zurich, Winterthurerstrasse 190, CH-8057, Zurich, Switzerland;

Ivan Corbeski - Department of Biochemistry, University of Zurich, Winterthurerstrasse 190, CH-8057, Zurich, Switzerland;

Valeria Romanucci - Università degli Studi di Napoli Federico II, Via Cintia 4, I-80126, Napoli, Italia

Giovanni Di Fabio - Università degli Studi di Napoli Federico II, Via Cintia 4, I-80126, Napoli, Italia

Author Contributions

§F.E. and A.I. contributed equally to this work. The manuscript was written through contributions of all authors. All authors have given approval to the final version of the manuscript.

Acknowledgments

We thank Thomas Frei (Department of Biochemistry, UZH) for assistance in cloning and protein expression and purification. This work was supported by the Swiss Cancer Research Foundation (grant number KFS 5748-02-2023 to AC) and the Swiss National Science Foundation (grant number 310030_212195 to AC).

References

- (1) Kumar, S.; Mohapatra, T. Deciphering Epitranscriptome: Modification of mRNA Bases Provides a New Perspective for Post-Transcriptional Regulation of Gene Expression. *Front Cell Dev Biol* **2021**, *9*, 628415. DOI: 10.3389/fcell.2021.628415.
- (2) Roignant, J. Y.; Soller, M. m⁶A in mRNA: An Ancient Mechanism for Fine-Tuning Gene Expression. *Trends in Genetics* **2017**, *33* (6), 380–390. DOI: 10.1016/j.tig.2017.04.003.
- (3) Boccaletto, P.; Stefaniak, F.; Ray, A.; Cappannini, A.; Mukherjee, S.; Purta E.; Kurkowska, M.; Shirvanizadeh, N.; Destefanis, E.; Groza, P.; Avşar G.; Romitelli, A.; Pir P., Dassi, E.; Conticello,

S. G.; Aguilo, F.; Bujnicki, J. M. MODOMICS: A Database of RNA Modification Pathways. 2021 Update. *Nucleic Acids Res* **2021**, *50*. DOI: 10.1093/nar/gkab1083

(4) Dominissini, D.; Moshitch-Moshkovitz, S.; Schwartz, S.; Salmon-Divon, M.; Ungar, L.; Osenberg, S.; Cesarkas, K.; Jacob-Hirsch, J.; Amariglio, N.; Kupiec, M.; Sorek, R.; Rechavi, G. Topology of the Human and Mouse m⁶A RNA Methylomes Revealed by m⁶A-Seq. **2012**, *485* (7397), 201–206. DOI: 10.1038/nature11112

(5) Alarcón, C. R.; Goodarzi, H.; Lee, H.; Liu, X.; Tavazoie, S.; Tavazoie, S. F. HNRNPA2B1 Is a Mediator of m⁶A-Dependent Nuclear RNA Processing Events. *Cell* **2015**, *162* (6), 1299–1308. DOI: 10.1016/j.cell.2015.08.011

(6) Li, A.; Chen, Y. S.; Ping, X. L.; Yang, X.; Xiao, W.; Yang, Y.; Sun, H. Y.; Zhu, Q.; Baidya, P.; Wang, X.; Bhattarai, D. P.; Zhao, Y. L.; Sun, B. F.; Yang, Y. G. Cytoplasmic m⁶A Reader YTHDF3 Promotes mRNA Translation. *Cell Research* **2017**, *27* (3), 444–447. DOI: 10.1038/cr.2017.10

(7) Wang, X.; Lu, Z.; Gomez, A.; Hon, G. C.; Yue, Y.; Han, D.; Fu, Y.; Parisien, M.; Dai, Q.; Jia, G.; Ren, B.; Pan, T.; He, C. N⁶-Methyladenosine-Dependent Regulation of Messenger RNA Stability. *Nature* **2013**, *505* (7481), 117–120. DOI: 10.1038/nature12730

(8) Xiao, W.; Adhikari, S.; Dahal, U.; Chen, Y. S.; Hao, Y. J.; Sun, B. F.; Sun, H. Y.; Li, A.; Ping, X. L.; Lai, W. Y.; Wang, X.; Ma, H. L.; Huang, C. M.; Yang, Y.; Huang, N.; Jiang, G. Bin; Wang, H. L.; Zhou, Q.; Wang, X. J.; Zhao, Y. L.; Yang, Y. G. Nuclear m⁶A Reader YTHDC1 Regulates mRNA Splicing. *Mol Cell* **2016**, *61* (4), 507–519. DOI: 10.1016/j.molcel.2016.01.012

(9) Shi, H.; Wang, X.; Lu, Z.; Zhao, B. S.; Ma, H.; Hsu, P. J.; Liu, C.; He, C. YTHDF3 Facilitates Translation and Decay of N⁶-Methyladenosine-Modified RNA. *Cell Res* **2017**, *27* (3), 315–328. DOI: 10.1038/cr.2017.15.

(10) Batista, P. J.; Giallourakis, C.; Correspondence, H. Y. C. m⁶A RNA Modification Controls Cell Fate Transition in Mammalian Embryonic Stem Cells. *Cell Stem Cell*, **2014**, *15* (6), 707–719. DOI: 10.1016/j.stem.2014.09.019

(11) Zhou, J.; Wan, J.; Gao, X.; Zhang, X.; Jaffrey, S. R.; Qian, S. B. Dynamic m⁶A mRNA Methylation Directs Translational Control of Heat Shock Response. *Nature* **2015**, *526* (7574), 591–594. DOI: 10.1038/nature15377

(12) Fustin, J. M.; Doi, M.; Yamaguchi, Y.; Hida, H.; Nishimura, S.; Yoshida, M.; Isagawa, T.; Morioka, M. S.; Kakeya, H.; Manabe, I.; Okamura, H. RNA-Methylation-Dependent RNA Processing Controls the Speed of the Circadian Clock. *Cell* **2013**, *155* (4), 793–806. DOI: 10.1016/j.cell.2013.10.026

(13) Barbieri, I.; Tzelepis, K.; Pandolfini, L.; Shi, J.; Millán-Zambrano, G.; Robson, S. C.; Aspris, D.; Migliori, V.; Bannister, A. J.; Han, N.; De Braekeleer, E.; Ponstingl, H.; Hendrick, A.; Vakoc, C. R.; Vassiliou, G. S.; Kouzarides, T. Promoter-Bound METTL3 Maintains Myeloid Leukaemia by m⁶A-Dependent Translation Control. *Nature* **2017**, *552* (7683), 126–131. DOI: 10.1038/nature24678

(14) Choe, J.; Lin, S.; Zhang, W.; Liu, Q.; Wang, L.; Ramirez-Moya, J.; Du, P.; Kim, W.; Tang, S.; Sliz, P.; Santisteban, P.; George, R. E.; Richards, W. G.; Wong, K. K.; Locker, N.; Slack, F. J.; Gregory, R. I. mRNA Circularization by METTL3–EIF3h Enhances Translation and Promotes Oncogenesis. *Nature* **2018**, *561* (7724), 556–560. DOI: 10.1038/s41586-018-0538-8

(15) Li, J.; Xie, H.; Ying, Y.; Chen, H.; Yan, H.; He, L.; Xu, M.; Xu, X.; Liang, Z.; Liu, B.; Wang, X.; Zheng, X.; Xie, L. YTHDF2 Mediates the mRNA Degradation of the Tumor Suppressors to Induce AKT Phosphorylation in N⁶-Methyladenosine-Dependent Way in Prostate Cancer. *Mol Cancer* **2020**, *19* (152). DOI: 10.1186/S12943-020-01267-6

(16) Cai, X.; Wang, X.; Cao, C.; Gao, Y.; Zhang, S.; Yang, Z.; Liu, Y.; Zhang, X.; Zhang, W.; Ye, L. HBXIP-Elevated Methyltransferase METTL3 Promotes the Progression of Breast Cancer via

- Inhibiting Tumor Suppressor Let-7g. *Cancer Lett* **2018**, *415*, 11–19. DOI: 10.1016/j.canlet.2017.11.018
- (17) Chen, M.; Wei, L.; Law, C. T.; Tsang, F. H.-C.; Shen, J.; Cheng, C. L.-H.; Tsang, L.-H.; Ho, D. W.-H.; Chiu, D. K.-C.; Lee, J. M.-F.; Wong, C. C.-L.; Ng, I. O.-L.; Wong, C.-M. RNA N6-Methyladenosine Methyltransferase-like 3 Promotes Liver Cancer Progression through YTHDF2-Dependent Posttranscriptional Silencing of SOCS2. *Hepatology* **2018**, *67* (6), 2254–2270. DOI: 10.1002/hep.29683
- (18) Zuo, X.; Chen, Z.; Gao, W.; Zhang, Y.; Wang, J.; Wang, J.; Cao, M.; Cai, J.; Wu, J.; Wang, X. M6A-Mediated Upregulation of LINC00958 Increases Lipogenesis and Acts as a Nanotherapeutic Target in Hepatocellular Carcinoma. *J Hematol Oncol* **2020**, *13* (5). DOI: 10.1186/s13045-019-0839-x
- (19) Shen, C.; Xuan, B.; Yan, T.; Ma, Y.; Xu, P.; Tian, X.; Zhang, X.; Cao, Y.; Ma, D.; Zhu, X.; Zhang, Y.; Fang, J. Y.; Chen, H.; Hong, J. m⁶A-Dependent Glycolysis Enhances Colorectal Cancer Progression. *Mol Cancer* **2020**, *19* (72). DOI: 10.1186/s12943-020-01190-w
- (20) Li, T.; Hu, P. S.; Zuo, Z.; Lin, J. F.; Li, X.; Wu, Q. N.; Chen, Z. H.; Zeng, Z. L.; Wang, F.; Zheng, J.; Chen, D.; Li, B.; Kang, T. B.; Xie, D.; Lin, D.; Ju, H. Q.; Xu, R. H. METTL3 Facilitates Tumor Progression via an m⁶A-IGF2BP2-Dependent Mechanism in Colorectal Carcinoma. *Mol Cancer* **2019**, *18* (112). DOI: 10.1186/s12943-019-1038-7
- (21) Ślędz, P.; Jinek, M. Structural Insights into the Molecular Mechanism of the m⁶A Writer Complex. *Elife* **2016**, *5*, e18434. DOI: 10.7554/eLife.18434
- (22) Wang, P.; Doxtader, K. A.; Nam, Y. Structural Basis for Cooperative Function of Mettl3 and Mettl14 Methyltransferases. *Mol Cell* **2016**, *63* (2), 306–317. DOI: 10.1016/j.molcel.2016.05.041
- (23) Sun, T.; Wu, R.; Ming, L. The Role of m⁶A RNA Methylation in Cancer. *Biomedicine & Pharmacotherapy* **2019**, *112*, 108613. DOI: 10.1016/j.biopha.2019.108613
- (24) Lin, S.; Choe, J.; Du, P.; Triboulet, R.; Gregory, R. I. The m⁶A Methyltransferase METTL3 Promotes Translation in Human Cancer Cells. *Mol Cell* **2016**, *62* (3), 335–345. DOI: 10.1016/j.molcel.2016.03.021
- (25) Dolbois, A.; Bedi, R. K.; Bochenkova, E.; Müller, A.; Moroz-Omori, E. V.; Huang, D.; Cafilisch, A. 1,4,9-Triazaspiro[5.5]Undecan-2-One Derivatives as Potent and Selective METTL3 Inhibitors. *J Med Chem* **2021**, *64* (17), 12738–12760. DOI: 10.1021/acs.jmedchem.1c00773
- (26) Moroz-Omori, E. V.; Huang, D.; Kumar Bedi, R.; Cheriya-kunnel, S. J.; Bochenkova, E.; Dolbois, A.; Rzczkowski, M. D.; Li, Y.; Wiedmer, L.; Cafilisch, A. METTL3 Inhibitors for Epitranscriptomic Modulation of Cellular Processes. *ChemMedChem* **2021**, *16* (19), 3035–3043. DOI: 10.1002/cmdc.202100291
- (27) Yankova, E.; Blackaby, W.; Albertella, M.; Rak, J.; De Braekeleer, E.; Tsagkogeorga, G.; Pilka, E. S.; Aspris, D.; Leggate, D.; Hendrick, A. G.; Webster, N. A.; Andrews, B.; Fosbeary, R.; Guest, P.; Irigoyen, N.; Eleftheriou, M.; Gozdecka, M.; Dias, J. M. L.; Bannister, A. J.; Vick, B.; Jeremias, I.; Vassiliou, G. S.; Rausch, O.; Tzelepis, K.; Kouzarides, T. Small-Molecule Inhibition of METTL3 as a Strategy against Myeloid Leukaemia. *Nature* **2021**, *593* (7860), 597–601. DOI: 10.1038/s41586-021-03536-w
- (28) Bedi, R. K.; Huang, D.; Li, Y.; Cafilisch, A. Structure-Based Design of Inhibitors of the m(6)A-RNA Writer Enzyme METTL3. *ACS bio & med chem Au* **2023**, *3* (4), 359–370. DOI: 10.1021/acsbiochemchem.3c00023
- (29) Finkelstein, J. D.; Martin, J. J. Methionine Metabolism in Mammals. Distribution of Homocysteine between Competing Pathways. *Journal of Biological Chemistry* **1984**, *259* (15), 9508–9513. DOI: 10.1016/S0021-9258(17)42728-1
- (30) Pei, H.; Peng, Y.; Zhao, Q.; Chen, Y. Small Molecule PROTACs: An Emerging Technology for Targeted Therapy in Drug Discovery. *RSC Adv* **2019**, *9* (30), 16967. DOI: 10.1039/c9ra03423d
- (31) Békés, M.; Langley, D. R.; Crews, C. M. PROTAC Targeted Protein Degraders: The Past Is Prologue. *Nature Reviews Drug Discovery* **2022**, *21*:3 **2022**, *21* (3), 181–200. DOI: 10.1038/s41573-021-00371-6
- (32) Zou, Y.; Ma, D.; Wang, Y. The PROTAC Technology in Drug Development. *Cell Biochem Funct* **2019**, *37* (1), 21–30. DOI: 10.1002/cbf.3369
- (33) Bond, M. J.; Crews, C. M. Proteolysis Targeting Chimeras (PROTACs) Come of Age: Entering the Third Decade of Targeted Protein Degradation. *RSC Chem Biol* **2021**, *2* (3), 725–742. DOI: 10.1039/d1cb00011j
- (34) Webb, T.; Craigon, C.; Ciulli, A. Targeting Epigenetic Modulators Using PROTAC Degraders: Current Status and Future Perspective. *Bioorg Med Chem Lett* **2022**, *63*, 128653. DOI: 10.1016/j.bmcl.2022.128653
- (35) Winter, G. E.; Buckley, D. L.; Paulk, J.; Roberts, J. M.; Souza, A.; Dhe-Paganon, S.; Bradner, J. E. Phthalimide Conjugation as a Strategy for in Vivo Target Protein Degradation. *Science* **2015**, *348* (6241), 1376–1381. DOI: 10.1126/science.aab1433
- (36) Han, X.; Zhao, L.; Xiang, W.; Qin, C.; Miao, B.; McEachern, D.; Wang, Y.; Metwally, H.; Wang, L.; Matvekas, A.; Wen, B.; Sun, D.; Wang, S. Strategies toward Discovery of Potent and Orally Bioavailable Proteolysis Targeting Chimera Degraders of Androgen Receptor for the Treatment of Prostate Cancer. *J Med Chem* **2021**, *64* (17), 12831–12854. DOI: 10.1021/acs.jmedchem.1c00882
- (37) Wiedmer, L.; Eberle, S. A.; Bedi, R. K.; Ślędz, P.; Cafilisch, A. A Reader-Based Assay for m⁶A Writers and Erasers. *Anal Chem* **2019**, *91* (4), 3078–3084. DOI: 10.1021/acs.analchem.8b05500
- (38) Troy Bemis, M. A.; La Clair, J. J.; Burkart, M. D. Unraveling the Role of Linker Design in Proteolysis Targeting Chimeras. *J Med Chem* **2021**, *64* (12), 8042–8052. DOI: 10.1021/acs.jmedchem.1c00482
- (39) Shi, Y.; Shi, B.; Dass, A. *et al.* Stable Upconversion Nanohybrid Particles for Specific Prostate Cancer Cell Immunodetection. *Sci Rep* **2016**, *6*, 37533. DOI: 10.1038/srep37533
- (40) Zhang, P.; Jain, P.; Tsao, C.; Wu, K.; Jiang, S. Proactively Reducing Anti-Drug Antibodies via Immunomodulatory Bioconjugation. *Angewandte Chemie* **2019**, *131* (8), 2455–2458. DOI: 10.1002/ange.201814275
- (41) Jones, M. W.; Strickland, R. A.; Schumacher, F. F.; Caddick, S.; Baker, J. R.; Gibson, M. I.; Haddleton, D. M. Polymeric Dibromomaleimides as Extremely Efficient Disulfide Bridging Bioconjugation and Pegylation Agents. *J Am Chem Soc* **2012**, *134* (3), 1847–1852. DOI: 10.1021/ja210335f
- (42) Han, B. A Suite of Mathematical Solutions to Describe Ternary Complex Formation and Their Application to Targeted Protein Degradation by Heterobifunctional Ligands. *Journal of Biological Chemistry* **2020**, *295* (45), 15280–15291. DOI: 10.1074/jbc.RA120.014715
- (43) Gadd, M.; Testa, A.; Lucas, X. *et al.* Structural basis of PROTAC cooperative recognition for selective protein degradation. *Nat Chem Biol* **2017**, *13*, 514–521. DOI: 10.1038/nchembio.2329
- (44) Sun, X.; Gao, H.; Yang, Y.; He, M.; Wu, Y.; Song, Y.; Tong, Y.; Rao, Y. PROTACs: Great Opportunities for Academia and Industry. *Signal Transduction and Targeted Therapy* **2019**, *4* (64). DOI: 10.1038/s41392-019-0101-6
- (45) Alshareef, A.; Zhang, HF.; Huang, YH. *et al.* The use of cellular thermal shift assay (CETSA) to study Crizotinib resistance in ALK-expressing human cancers. *Sci Rep* **2016**, *6*, 33710. DOI: 10.1038/srep33710

- (46) Borsari, C.; Trader, D. J.; Tait, A.; Costi, M. P. Designing Chimeric Molecules for Drug Discovery by Leveraging Chemical Biology. *J Med Chem* **2020**, *63* (5), 1908–1928. DOI: 10.1021/acs.jmedchem.9b01456
- (47) Hendrick, C. E.; Jorgensen, J. R.; Chaudhry, C.; Strambeanu, I. I.; Brazeau, J. F.; Schiffer, J.; Shi, Z.; Venable, J. D.; Wolkenberg, S. E. Direct-to-Biology Accelerates PROTAC Synthesis and the Evaluation of Linker Effects on Permeability and Degradation. *ACS Med Chem Lett* **2022**, *13* (7), 1182–1190. DOI: 10.1021/acsmchemlett.2c00124
- (48) Donoghue, C.; Cubillos-Rojas, M.; Gutierrez-Prat, N.; Sanchez-Zarzalejo, C.; Verdaguer, X.; Riera, A.; Nebreda, A. R. Optimal Linker Length for Small Molecule PROTACs That Selectively Target P38a and P38b for Degradation. *Eur J Med Chem* **2020**, *201*, 112451. DOI: 10.1016/j.ejmech.2020.112451
- (49) Liu, X.; Kalogeropoulou, A. F.; Domingos, S.; Makukhin, N.; Nirujogi, R. S.; Singh, F.; Shpiro, N.; Saalfrank, A.; Sammler, E.; Ganley, I. G.; Moreira, R.; Alessi, D. R.; Ciulli, A. Discovery of XL01126: A Potent, Fast, Cooperative, Selective, Orally Bioavailable, and Blood-Brain Barrier Penetrant PROTAC Degradator of Leucine-Rich Repeat Kinase 2. *J Am Chem Soc* **2022**, *144* (37), 16930–16952. DOI: 10.1021/jacs.2c05499
- (50) Xiang, W.; Zhao, L.; Han, X.; Xu, T.; Kregel, S.; Wang, M.; Miao, B.; Qin, C.; Wang, M.; McEachern, D.; Lu, J.; Bai, L.; Yang, C. Y.; Kirchhoff, P. D.; Takyi-Williams, J.; Wang, L.; Wen, B.; Sun, D.; Ator, M.; Mckean, R.; Chinnaiyan, A. M.; Wang, S. Discovery of ARD-1676 as a Highly Potent and Orally Efficacious AR PROTAC Degradator with a Broad Activity against AR Mutants for the Treatment of AR + Human Prostate Cancer. *J Med Chem* **2023**, *66* (18), 13280–13303. DOI: 10.1021/acs.jmedchem.3c01264
- (51) García Jiménez, D.; Rossi Sebastiano, M.; Vallaro, M.; Mileo, V.; Pizzirani, D.; Moretti, E.; Ermondi, G.; Caron, G. Designing Soluble PROTACs: Strategies and Preliminary Guidelines. *J Med Chem* **2022**, *65* (19), 12639–12649. DOI: 10.1021/acs.jmedchem.2c00201
- (52) Khan, S.; He, Y.; Zhang, X.; Yuan, Y.; Pu, S.; Kong, Q.; Zheng, G.; Zhou, D. PROteolysis Targeting Chimeras (PROTACs) as Emerging Anticancer Therapeutics. *Oncogene* **2020**, *39*, 4909–4924. DOI: 10.1038/s41388-020-1336-y
- (53) Desantis, J.; Mammoli, A.; Eleuteri, M.; Coletti, A.; Croci, F.; Macchiarulo, A.; Goracci, L. PROTACs bearing piperazine-containing linkers: what effect on their protonation state?. *RSC Adv* **2022**, *12*, 21968–21977. DOI: 10.1039/d2ra03761k
- (54) Han, X.; Zhao, L.; Xiang, W.; Miao, B.; Qin, C.; Wang, M.; Xu, T.; McEachern, D.; Lu, J.; Wang, Y.; Metwally, H.; Yang, C. Y.; Kirchhoff, P. D.; Wang, L.; Matvekas, A.; Takyi-Williams, J.; Wen, B.; Sun, D.; Ator, M.; Mckean, R.; Wang, S. Discovery of ARD-2051 as a Potent and Orally Efficacious Proteolysis Targeting Chimera (PROTAC) Degradator of Androgen Receptor for the Treatment of Advanced Prostate Cancer. *J Med Chem* **2023**, *66* (13), 8822–8843. DOI: 10.1021/acs.jmedchem.3c00405
- (55) Li, K.; Crews, C. M. PROTACs: Past, Present and Future. *Chem. Soc. Rev* **2022**, *51* (12), 5214–5236. DOI: 10.1039/d2cs00193d
- (56) Li, Y.; He, X.; Lu, X.; Gong, Z.; Li, Q.; Zhang, L.; Yang, R.; Wu, C.; Huang, J.; Ding, J.; He, Y.; Liu, W.; Chen, C.; Cao, B.; Zhou, D.; Shi, Y.; Chen, J.; Wang, C.; Zhang, S.; Zhang, J.; Ye, J.; You, H. METTL3 Acetylation Impedes Cancer Metastasis via Fine-Tuning Its Nuclear and Cytosolic Functions. *Nat Commun* **2022**, *13* (6350). DOI: 10.1038/s41467-022-34209-5
- (57) Yuan, Y.; Du, Y.; Wang, L.; Liu, X. The M6A Methyltransferase METTL3 Promotes the Development and Progression of Prostate Carcinoma via Mediating MYC Methylation. *J Cancer* **2020**, *11* (12), 3588–3595. DOI: 10.7150/jca.42338
- (58) Zhang, N.; Hou, D.; Hu, X.; Liang, J.; Wang, M.; Song, Z.; Yi, L.; Wang, Z.; An, H.; Xu, W.; Wang, H. Nano Proteolysis Targeting Chimeras (PROTACs) with Anti-Hook Effect for Tumor Therapy. *Angewandte Chemie* **2023**, *135* (37), e202308049. DOI: 10.1002/ange.202308049
- (59) Casement, R.; Bond, A.; Craigon, C.; Ciulli, A. Mechanistic and Structural Features of PROTAC Ternary Complexes. *Methods in Molecular Biology* **2021**, *2365*, 79–113. DOI: 10.1007/978-1-0716-1665-9_5
- (60) Xiao, H.; Zhao, R.; Meng, W.; Liao, Y. Effects and Translational Characteristics of a Small-Molecule Inhibitor of METTL3 against Non-Small Cell Lung Cancer. *J Pharm Anal* **2023**, *13* (6), 625–639. DOI: 10.1016/j.jppha.2023.04.009
- (61) Fischer, E. S.; Böhm, K.; Lydeard, J. R.; Yang, H.; Stadler, M. B.; Cavadini, S.; Nagel, J.; Serluca, F.; Acker, V.; Lingaraju, G. M.; Tichkule, R. B.; Schebesta, M.; Forrester, W. C.; Schirle, M.; Has-siepen, U.; Ottl, J.; Hild, M.; Beckwith, R. E. J.; Harper, J. W.; Jenkins, J. L.; Thomä, N. H. Structure of the DDB1-CRBN E3 Ubiquitin Ligase in Complex with Thalidomide. *Nature* **2014**, *512*, 49–53. DOI: 10.1038/nature13527
- (62) Xie, S.; Sun, Y.; Liu, Y.; Li, X.; Li, X.; Zhong, W.; Zhan, F.; Zhu, J.; Yao, H.; Yang, D. H.; Chen, Z. S.; Xu, J.; Xu, S. Development of Alectinib-Based PROTACs as Novel Potent Degradators of Anaplastic Lymphoma Kinase (ALK). *J Med Chem* **2021**, *64* (13), 9120–9140. DOI: 10.1021/acs.jmedchem.1c00270
- (63) Toure, M.; Crews, C. M. Small-Molecule PROTACs: New Approaches to Protein Degradation. *Angewandte Chemie International Edition* **2016**, *55* (6), 1966–1973. DOI: 10.1002/anie.201507978
- (64) Zeng, Z.-C.; Pan, Q.; Sun, Y.-M.; Huang, H.-J.; Chen, X.-T.; Chen, T.-Q.; He, B.; Ye, H.; Zhu, S.-X.; Pu, K.-J.; Fang, K.; Huang, W.; Chen, Y.-Q.; Wang, W.-T. METTL3 Protects METTL14 from STUB1-Mediated Degradation to Maintain m⁶A Homeostasis. *EMBO Rep* **2023**, *24* (3), e55762. DOI: 10.15252/embr.202255762
- (65) Hanthorn, J. J.; Valgimigli, L.; Pratt, D. A. Preparation of Highly Reactive Pyridine-and Pyrimidine-Containing Diarylamine Antioxidants. *J. Org. Chem.* **2012**, *77* (16), 6908–6916. DOI: 10.1021/jo301012x
- (66) Zhang, W.; Li, P.; Sun, S.; Jia, C.; Yang, N.; Zhuang, X.; Zheng, Z.; Li, S. Discovery of Highly Potent and Selective CRBN-Recruiting EGFR L858R/T790M Degradators in Vivo. *Eur J Med Chem* **2022**, *238*, 114509. DOI: 10.1016/j.ejmech.2022.114509
- (67) Zhang, H.; Zhao, H.-Y.; Xi, X.-X.; Liu, Y.-J.; Xin, M.; Mao, S.; Zhang, J.-J.; Lu, A.-X.; Zhang, S.-Q. Discovery of Potent Epidermal Growth Factor Receptor (EGFR) Degradators by Proteolysis Targeting Chimera (PROTAC). *Eur. J. Med. Chem.* **2020**, *208*, 112781. DOI: 10.1016/j.ejmech.2020.112061
- (68) Brownsey, D. K.; Rowley, B. C.; Gorobets, E.; Gelfand, B. S.; Derksen, D. J. Rapid Synthesis of Pomalidomide-Conjugates for the Development of Protein Degradator Libraries. *Chem. Sci.* **2021**, *12*, 4519–4525. DOI: 10.1039/d0sc05442a
- (69) Liu, J.; Yuan, L.; Ruan, Y.; Deng, B.; Yang, Z.; Ren, Y.; Li, L.; Liu, T.; Zhao, H.; Mai, R.; Chen, J. Novel CRBN-Recruiting Proteolysis-Targeting Chimeras as Degradators of Stimulator of Interferon Genes with In Vivo Anti-Inflammatory Efficacy. *J. Med. Chem* **2022**, *65* (9), 6593–6611. DOI: 10.1021/acs.jmedchem.1c01948
- (70) Gradia, S. D.; Ishida, J. P.; Tsai, M.-S.; Jeans, C.; Tainer, J. A.; Fuss, J. O. MacroBac: New Technologies for Robust and Efficient Large-Scale Production of Recombinant Multiprotein Complexes. *Methods in Enzymology* **2017**, *592*, 1–26. DOI: 10.1016/bs.mie.2017.03.008